



**Politecnico
di Torino**

POLITECNICO DI TORINO

Corso di Laurea Magistrale in ingegneria aerospaziale

A.a. 2020/2021

Sessione di Laurea Luglio 2021

Development of an experimental test bench for the validation of prognostic algorithms for electromechanical actuators

Relatori

Ing. Matteo Davide Lorenzo Dalla Vedova

Prof. Paolo Maggiore

Ing. Pier Carlo Berri

Candidato

Luca Boggio



Index

Index of figure	5
Abstract	7
More electric aircrafts	8
Flight control systems	12
Primary flight controls	14
Secondary flight control	17
Actuators	18
Electro-mechanic actuator	19
Hydro-mechanical Actuators	21
Electro-hydraulic Actuators	23
Electric motors	25
Lorentz Law	26
Brush/Brushless motors	27
Planetary gearbox	29
Opposing load vs aiding load	32
Backlash	36
Test bench overview	41
Introduction	41
SINAMICS Control Unit - CU310-2	44
Simatic Microbox PC	45
SINAMICS PM 240-2 Power module	46
Motor	47
Encoder	50
Brake module	51
Trigger System	52
Quick guideline for test bench	54
Introduction	54
Turn on test bench and hardware connections	55
Software connection: Starter to test bench	56
How to set and start test bench using Web server	56
How to set commands	58
How to enable commands	58

How to start running test bench	59
How to shut down test bench.....	60
HF model of electromechanics actuator.....	60
Command generation.....	61
Load generation – Load Cell values fitting	62
Control electronics (PID).....	63
Proportional branch.....	64
Integrative branch	65
Derivative branch.....	66
Inverter Model	66
Evaluation of phase currents	68
Hysteresis PWM	69
3-phase bridge.....	71
Electromagnetic model	72
Computation of back-EMF coefficients.....	73
Three phase RL model	77
Computation of motor torque.....	77
Material for stator and rotor	78
motor-transmission dynamical model	80
Borello friction model.....	81
Signal acquisition	84
Modification of parameters	84
Backlash evaluation.....	87
Testing campaign	89
Results	90
Variable load test campaign	97
Future trends.....	99
Bibliography.....	100

Index of figure

Figure 1: Estimate percentage delivered units.	8
Figure 2: Fleet in service expected to more than double over the next 20 years.	9
Figure 3: Electrical power evolution.	10
Figure 4: A380 control surfaces (green squares are hydraulic actuation).....	11
Figure 5: Consequences of actuation of flight controls.....	12
Figure 6: Primary and secondary flight controls.	14
Figure 7: Elevons location and working principles.....	16
Figure 8: Canard configuration.	17
Figure 9: Trimmable horizontal stabilizer.....	18
Figure 10: Scheme of an: a) EHA - b) EMA - c) HSA.	19
Figure 11: From left to right Geared EMA, Direct Drive EMA and Rotary EMA. LVDT: linear variable differential transformer.	21
Figure 12: Hydro-mechanical actuation.	22
Figure 13: Block diagram of electrohydraulic actuator.	23
Figure 14: Flapper-nozzle valve.....	24
Figure 15: Jet-pipe valve.	25
Figure 16: Electric motors classification.....	25
Figure 17: Scheme of a DC motor.	27
Figure 18: Trapezoidal control motor.	28
Figure 19: Motor-Gerabox-User diagram.	30
Figure 20: Detail of planetary gearbox.	31
Figure 21: Rotating wheels.	32
Figure 22: Simplified scheme of a reducer a).	33
Figure 23: Simplified scheme of a reducer b).	35
Figure 24: Lubrification regimes.....	37
Figure 25: Gear backlash definition.	38
Figure 26: "Backlash caused by center distance change: left: mated teeth before and after increase of center distance, Right: enlarge view of profiles and backlash ".	39
Figure 27: Backlash block.....	40
Figure 28: Gearbox - encoder assembly.....	41
Figure 29: Test bench.	42
Figure 30: Test bench diagram connections.....	43
Figure 31: Control Unit.....	44
Figure 32: Microbox PC with on the top the license key.....	45
Figure 33: Inverter PM 240-2.....	46
Figure 34: Inverter data.	47
Figure 35: SIMOTICS S synchronous motor.....	48
Figure 36: Encoder.	50
Figure 37: Braking module.	52
Figure 38: Electrical scheme for trigger switching.	53
Figure 39: Configuration of transistors.	53
Figure 40: Test bench connections.....	55
Figure 41: Web server main screen.....	57
Figure 42: Main menu.	57
Figure 43: Set commands window.	58
Figure 44: Enable command window.....	59
Figure 45: Start and Stop window.....	59
Figure 46: High-Fidelity Simulink model.....	61

Figure 47: Command block.....	62
Figure 48: Load Cells values input block.....	62
Figure 49: "Control Electronics (PID) subsystem."	63
Figure 50: PID subsystem.	64
Figure 51: Proportional gain.	65
Figure 52: Root locus transfer function.....	66
Figure 53: Inverter Inputs and Outputs.	67
Figure 54: Inverter model subsystem.	67
Figure 55: Reverse Park-Clarke transformation.....	68
Figure 56: Hysteresis subsystem.	70
Figure 57: Duty cycles examples.	71
Figure 58: 3-Phase bridge.	72
Figure 59: BLDC Electromagnetic model subsystem.....	73
Figure 60: Computation of back-EMF subsystem.	74
Figure 61: Electrical angular position.	74
Figure 62: Static rotor eccentricity.....	75
Figure 63: Dynamic rotor eccentricity.	76
Figure 64: three phase RL subsystem.	77
Figure 65: Computation of motor torque.	78
Figure 66: Hysteresis cycle of ferromagnetic materials.....	80
Figure 67: Motor-transmission dynamical model.	81
Figure 68: Borello's friction model.	83
Figure 69: Reaction model.	83
Figure 70: Signal acquisition blocks.	84
Figure 71: Modified Proportional gain.....	85
Figure 72: Modified Speed reference limiter.	86
Figure 73: Modified Current Reference limiter.	86
Figure 74: User inertia moment.	87
Figure 75: Comparison between calculated and experimental gear backlash.	89
Figure 76: Simulink, Test bench and command encoder position.	91
Figure 77: Differences between test bench and Simulink model.....	92
Figure 78: Comparison of motor positions.	92
Figure 79: Above Encoder with zero backlash and below planetary gearbox with maximum gear backlash.	94
Figure 80: Position Encoder error.	95
Figure 81: Position motor error.	95
Figure 82: Speed comparisons.	96
Figure 83: Minimum, medium and maximum gear backlash on last stage of the planetary gearbox.	97
Figure 84: Linear distribution of torque tests.....	98

Abstract

From 2000 to today, air traffic due to civil aviation has seen an increase of 2.4 times, and with a forecast of doubling further in 15 years. The growth of the aerospace industry leads to raise up standards and considers cost effective solution. Electromechanical actuators in the last century have a high growth rate. These parts will become essential for primary and secondary flight controls, this transition leads to higher quality standards and the development of algorithms that can predict their operation.

Through prognostics algorithms it will be possible to evaluate in real time the behavior of the aircraft and predict failures. An important problem is maintenance, with the use of these algorithms it will be possible to schedule and optimize maintenance using real-time data and models to reproduce actuators behavior.

The initial aim of the thesis in the development of an experimental test bench is to develop and create a test bench to validate the prognostics models.

The development of the test bench consisted of several stages; first an analysis and design of major parts, then the assembly of the test bench. The last step to complete the test bench is to characterize the components and to achieve the desired results.

The test bench consists of an electric brushless motor, a planetary gearbox, a braking system, a motor actuation and control system, an encoder for closed loop and an Arduino board for brake control.

In this thesis, the electromechanical actuator test bench is adapted to the requirements. In particular, after the characterizations carried out in previous works, it was possibly make tests on different ways:

- Variable backlash with zero load: backlash was inserted on the user.
- Load variation and backlash variation: application of load on the motor shaft with variable backlash.

The development of prognostication algorithms (HF model) was carried out in the MatLab/Simulink environment. The model used takes into account the main physical effects present in the test bench.

Using Simulink, the electromagnetic model of the motor, the model of the inverter controlling the electric motor, the control electronics and the planetary transmission were modelled. Simulink model takes into account also:

- Friction effects by Borello's friction model.
- Include a short-circuit on each phase of the electric motor.
- Some hysteresis effects.

The validation of the prognostics algorithms was carried out by evaluating the data obtained with the bench test with those of the Simulink model. The comparison and validation of prognostics algorithms made it necessary to calibrate the Simulink model in order to better simulate the behavior of the test bench; this work made it possible to study and validate the backlash model implemented in the Simulink model.

More electric aircrafts

Aerospace and defense are the main sector of research and develop, through years a lot of engineering solution come from aeronautic or space. Engineering, on this sense, found fertile ground in develop newest ideas and advanced solution for customers satisfaction.

From 2000 to today, air traffic due to civil aviation has seen an increase of 2.4 times, and with a forecast of doubling further in 15 years. In the next twenty years civil aviation aircrafts delivered will reached 40000 units; a part of this vehicles will replace oldest vehicle which are at the end of life, another part of this units will used to improve aerospace sector develop.

	2019-2028	2028-2038	2019-2038	SHARE OF 2019-2038 NEW DELIVERIES
AFRICA	520	750	1,270	3%
ASIA-PACIFIC	6,500	10,040	16,540	42%
CIS	700	840	1,540	4%
EUROPE	3,790	3,750	7,540	19%
LATIN AMERICA	1,330	1,370	2,700	7%
MIDDLE EAST	1,410	1,830	3,240	8%
NORTH AMERICA	3,330	3,050	6,380	17%
WORLD TOTAL	17,580	21,630	39,210	100%

Figure 1: Estimate percentage delivered units.

Nowadays 40% of passengers of all the world pass through one of the 66 AMC cities (those cities are the Aviation Mega Cities), they are large enough to have an airport, these phenomena will increase with the cities growth and the amount will increase to 95 in the next twenty years. Aircrafts transport will increase, and technology will need to be improved.

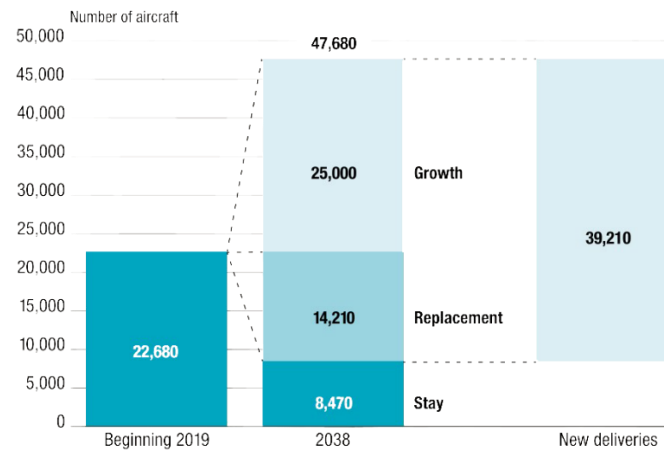


Figure 2: Fleet in service expected to more than double over the next 20 years.

Innovative approaches and algorithm of optimization will be reliable and powerful on this sense technology has the main role in particular the electric control is one of the most growing sectors. The continuous growth of air traffic has also brought to light a new problem: the environmental issue. the growth of pollutants in the air has led to the adoption of less polluting solutions also in the aerospace sector *“It is often claimed that 1 kg saved on each flight could save roughly 1,700 t of fuel and 5,400 t of CO₂ per year for all air traffic”* this is an important fact and the possibility of reducing CO₂ emissions is possible by lightening the aircraft.

Convectional aircrafts are drive by some energy:

- Electrical: on board systems, avionic, light, battery and de-icing system.
- Pneumatic: air conditioning, deicing
- Hydraulic: primary and secondary controls)
- Mechanical: broadcast forces, is combine with hydraulic system, gearboxes.
- Fuel: provide the energy to feed turbines.

Engineers to save weight replaced some pneumatic or hydraulic systems with electrical

system, that fact is possible to see in the figure below:

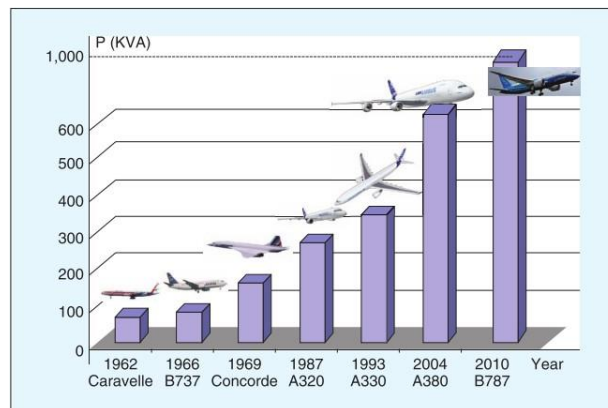


Figure 3: Electrical power evolution.

During the sixties, aircraft do not have an advanced electrical system. For example, Boeing 737 has primary electrical power is generated by two generators which are drive by turbines, the electrical generation is provide with three phase, 400 Hz and 115 Volt. The APU is used on ground and when the main two generators mounted on each engine are inoperative. The electrical system on this aircraft is used to provide computers, galleys, on-board devices, lights, and recharge battery; is clear the electrical system is necessary but is not the largest system.

Over the time, the electrical power mounted increased by almost 100 KVA up to 1000 KVA during 2010, this is a clear signal that the electrical system plays a major role and more and more systems are replaced by electrical system.

Replacing with electrical system is due to a rationalization of the powers and therefore to a better management of the electric all powers. During aircraft life cycle there are direct costs, which include fuel, crew and acquisition costs; indirect costs are related to the support of the structure that provides for the management of the aircraft and costs related to maintenance. A replacement of the hydraulic technology with an electrical-only technology will bring the availability and especially the ability to easily isolate the failure and prevent the damage from spreading to other systems.

Hydraulic systems do not allow the isolation of the failure. During fault condition the loss of an actuator leads to the isolation of the entire circuit. In the future through neural algorithms will be possible to predict failures through a real-time monitoring of aircraft condition.

One of the most important purpose of this thesis is to proceed on this path, going to study algorithms that can simulate the operating conditions of an electromechanical actuation system in order to reproduce in a realistic way the behavior of the systems.

The replacement of hydraulic actuation can also take place in the ground segment. Starting and testing systems (such as actuations for cabin pressure tests or material loading/unloading systems). On the other hand, the use of an electric system for the landing gear offers the possibility to add an electric motorization to the wheels and this leads to the reduction of consumption; the actuation of the wheels of the landing gear leads to have the motors at low revolutions and a consequent reduction of consumption and CO2 emissions.

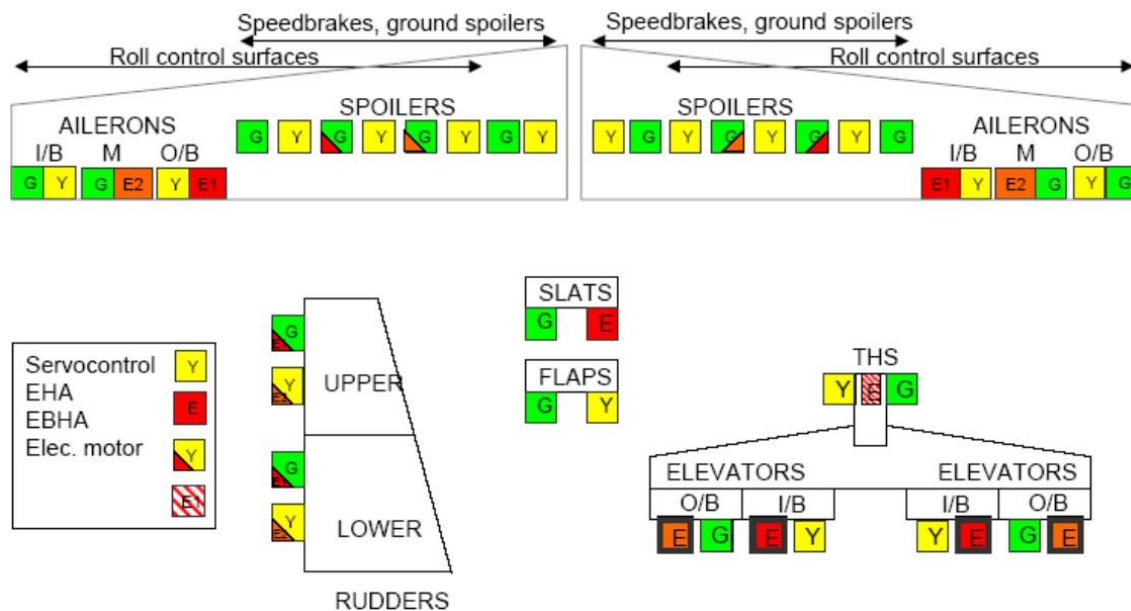


Figure 4: A380 control surfaces (green squares are hydraulic actuation)

The modern trend has led to have higher electrical powers incorporated on aircrafts. Although the probability that the total mass may increase, but the major advantages are concentrated in the rationalization of electrical powers and in the management capacity. Another important aspect lies in maintenance.

Maintenance costs can be reduced considerably and could be transformed into just monitoring the health of the system. these monitoring systems can have a dual function. First is to be able to identify the state of degradation of the aircraft and then adjust maintenance plan optimized for each aircraft; second is through a monitoring of the system in all its parts

offers the possibility to obtain a command with different actuations; this possibility makes the system adaptable to various operating conditions and especially offers the possibility to obtain the same result using different components (in the case of flight controls for example). This methodology from one side controls which components are deteriorating first and after an evaluation tries to obtain the same result using less worn components. The result of this technique is reflected in less frequent maintenance and an optimized scheduling.

Flight control systems

In order to be able to move in space and to be controlled, an aircraft needs a control system (Flight control System - FCS).

The control system of an aircraft consists of many elements that perform different functions, but all have the same purpose, that of locally modifying the aerodynamic forces through the variation of the external shape of the aircraft. The following diagram shows the effect of implementing a flight command.

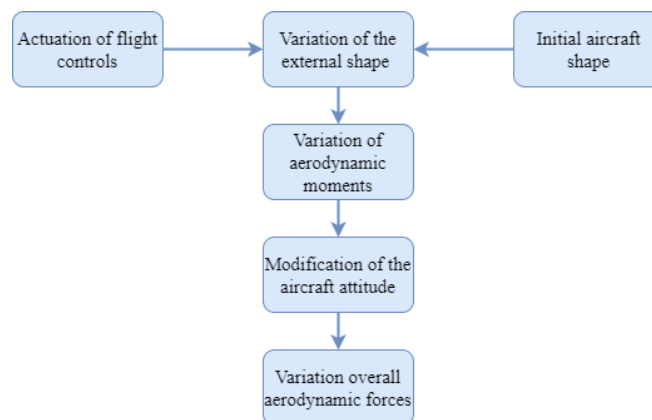


Figure 5: Consequences of actuation of flight controls.

flight controls must meet three important requirements:

- Instinctiveness
- Sensitivity
- Stability

Must be instinctive in order to provide the pilot with the correct sensations during manoeuvres; for example, if the pilot tilts the control stick to the left, the aircraft must create a configuration change in order to rotate around the longitudinal axis. Sensitivity is a ratio between a sensor measurement and the corresponding actual physical quantity. Sensitivity in flight controls is essential in order to be able to control the actuation of moving surfaces in a regular and precise manner. Oscillations due to gusts or external controls must comply with the requirements of the regulations in order to avoid making the aircraft unstable.

Flight control performance is expressed by two main parameters:

- The stall load.
- The no-load actuation speed.

The first is the maximum load the structure can bear, i.e., the maximum hinge moment, while the no-load actuation speed can be measured at zero load. The requirements on primary and secondary flight controls are different; for secondary flight controls the stall load is 1,5 times the maximum load; for primary flight controls the stall load is defined as twice the maximum load. The stricter requirement on primary flight controls is due to the fact that the load affects the actuation speed negatively, in primary flight controls a slowing down of the control is avoided. Generally, no-load actuation speeds reach $60^\circ/sec$ while secondary flight controls $6^\circ/sec$ for secondary flight controls assisting primary flight controls actuation speeds are $15^\circ/sec$.

Primary flight control and secondary flight control are different and are located on the wing and tail of aircraft.

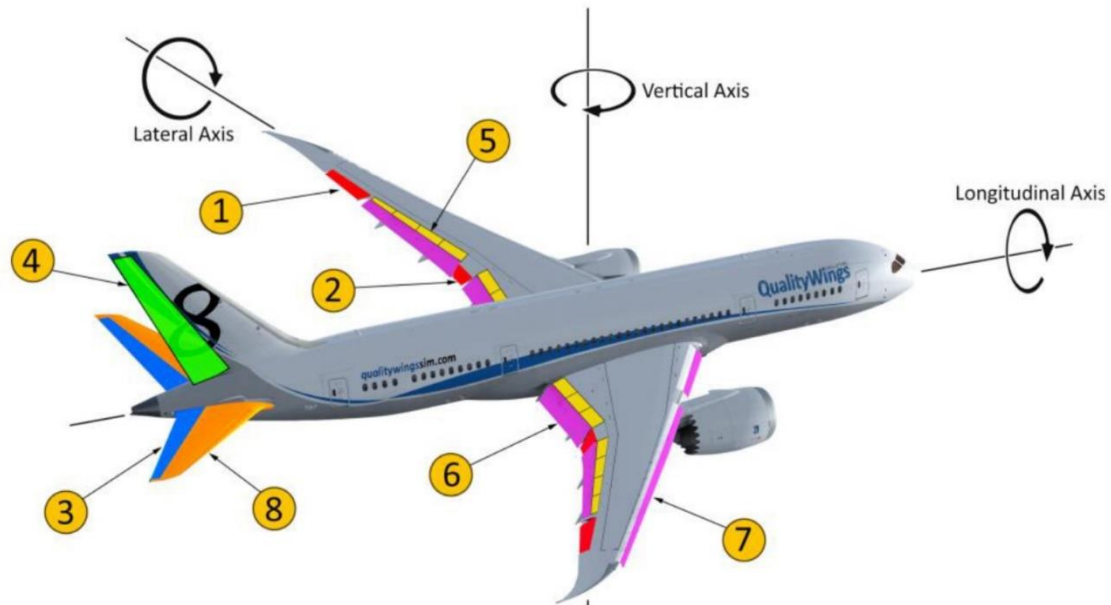


Figure 6: Primary and secondary flight controls.

Primary flight controls

The state of the art of primary flight controls is that there are three categories:

- Fully mechanic flight controls, they are used for small aircraft and gliders, these controls are also called “reversible” and uses with a mechanical transmission.
- Servocontrols with hydraulically feed for large aircraft, this solution is combined with a fly-by-wire technology.
- Servocontrols with hydraulically feed for medium aircraft
- Servocontrols with electrical feed, this solution is now used only for backup command.

Looking at the figure above, the primary flight controls are located at numbers 1, 3, 4.

1—Ailerons

- The ailerons are located at the end of each wing.
- Their role is to create a moment around the longitudinal axis of the aircraft.
- Their implementation is anti-symmetrical to create two concordant moments.
- Ailerons creates the "*Rolling moment*".

2—Elevators

- Elevons are one for each horizontal stabilizer and move together.
- They create a momentum around the aircraft's center of gravity and a rotation around the lateral axis.
- Elevons lower or raise the aircraft; they can be controlled by either the pilot or the autopilot.

4— Rudder

- Rudder provide yaw control.
- During takeoff, the rudder becomes aerodynamically effective at approximately 60 knots groundspeed if not activated by the pilot.
- Rudder creates a momentum around the vertical axis.

In addition to the normal primary flight controls, there are also some controls that are secondary but can act as primary flight controls:

5— Spoiler (flight spoilers)

- spoilers increase the effect of aileron activations if operated asymmetrically, if spoilers are operated symmetrically, they can act as speed brakes
- Creating increased resistance and decreased sustenance.

In addition to the usual primary control configurations, you can also find other configurations depending on the type of aircraft you are considering. it is possible to group the primary flight controls into three other families:

— Elevon

These controls are used in military aircraft and are positioned on the trailing edge. this configuration is usually adopted in delta-wing aircraft. the principle of operation of the elevons is to combine the effects of ailerons and elevator without the use of a horizontal tail surface.

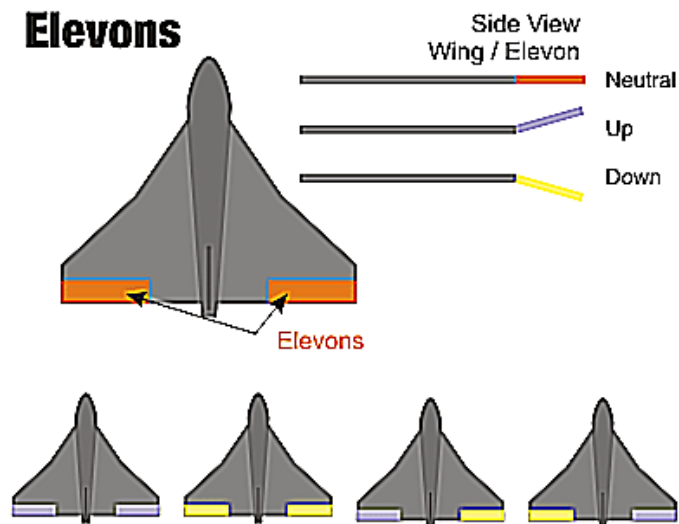


Figure 7: Elevons location and working principles.

2— Flaperon

these controls can be found on airliners and are inserted in the middle of the flaps these surfaces are fixed to the trailing edge of the aircraft and can be used either symmetrically or asymmetrically

— Canard

This particular configuration involves the positioning of horizontal load-bearing surfaces on the nose of the aircraft (Piaggio P180 configuration).

Aircraft of this type have a wing that is very far back with respect to the center of gravity; the advantage of adopting this configuration lies in the fact that the aircraft has a very fast response to manoeuvres, because the canard post on the nose to carry out a flare contributes positively to the total lift.

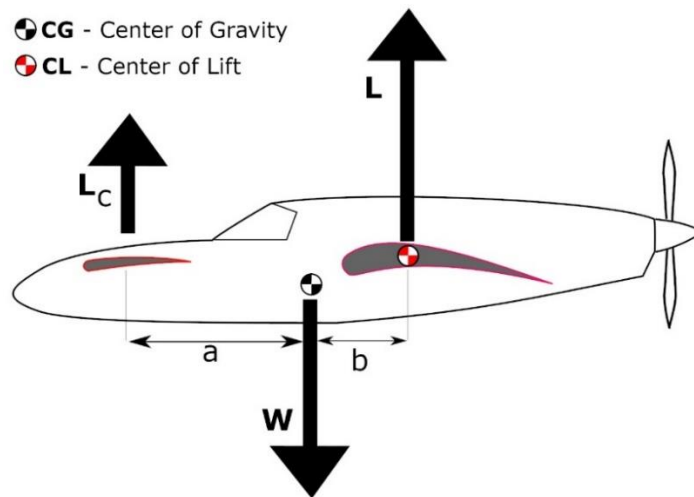


Figure 8: Canard configuration.

Secondary flight control

6— Flaps

- These surfaces are installed on the trailing edge.
- Flaps are generally used during take-off and landing manoeuvres.
- They create a high lift and on large aircraft can significantly increase the wing area; a consequence of this is a decrease in landing speed and a shorter take-off length.

6— Slats

- These surfaces are installed on the leading edge.
- Slats are generally used during take-off and landing manoeuvres.
- They create a high lift and on large aircraft can significantly increase the wing area; a consequence of this is a decrease in landing speed and a shorter take-off length.

5— Spoilers and speedbrakers

- Their function is to increase drag in order to slow down the aircraft.
- They can also be used as primary flight controls.

8— Horizontal Stabilizer Trim

- the stabilizer in large aircraft has the ability to rotate on itself and therefore to be "trimmable". this solution is adopted to reduce the pilot's workload.

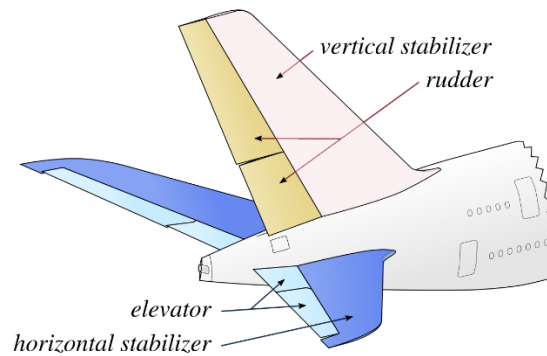


Figure 9: Trimmable horizontal stabilizer.

Actuators

The new concept of the "*more electric*" aircraft has allowed a considerable development of these systems; there are many advantages, the absence of a fluid transmitting motion offers the possibility to avoid oil leaks and the consequent damage of the system or other systems. The absence of fluid also allows the isolation of the fault without damaging the entire command line; a major problem in the aerospace sector is maintenance, the adoption of electromechanical systems allows faster and easier maintenance as the command transmission line is composed only of electrical cables, most maintenance work can be concentrated only in the area of the actuator. The electromechanical actuator transports the power in cables between the devices, controls with hydraulic actuations use line pipes. At the state of the art electromechanical actuators are used as primary flight controls only by military aircraft, while in commercial aircraft they are limited to secondary flight controls, brakes and horizontal stabilizer in the Boeing 787.

The figure below compares actuators families:

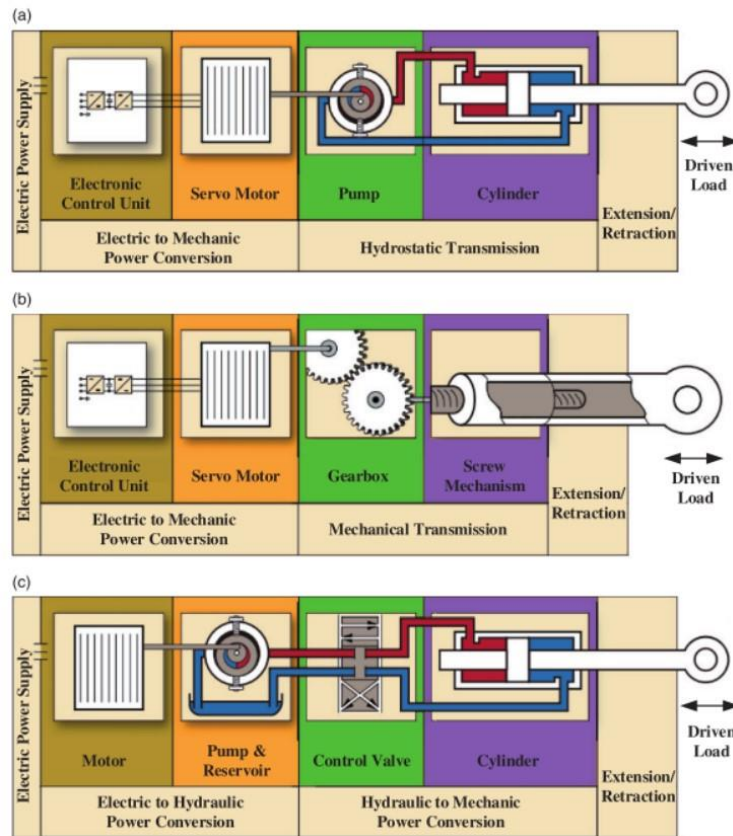


Figure 10: Scheme of an: a) EHA - b) EMA - c) HSA.

Figure 10 a) represents an electro-hydrostatic actuator, these actuators are servomotors controlling a hydraulic pump which provides for the actuation of the load. Figure 10 b) represents the electro-mechanical actuators which are composed of an electric motor, box gears and control electronics. finally, Figure 10 c) represents the hydraulic servo actuators which are activated by an electric motor which controls an electro-hydraulic valve.

Electro-mechanic actuator

Electromechanical actuators are devices used for precision actuations. These devices consist of an electric motor and a motion transmission system such as a gearbox.

In many cases electromechanical actuators are combined with gearboxes with a high transmission ratio. For flight controls, the rotational speed of the electric motor relative to the rotational speed of the user is about an order of magnitude higher. The transmission ratio

can be expressed according to the usual laws of mechanics, where T represent the transmission ratio.

$$\tau = \frac{\omega_m}{\omega_u} = \frac{Torque_u}{\eta_m \cdot Torque_u}$$

By the expression above ω_u and ω_m are respectively the angular speeds of user and angular speeds of motor, on the other hand η_m represent the mechanical transmission efficiency.

Electromechanical actuation is used to:

- Move flight surfaces
- Stabilize and aim rotating devices
- Steer antennas
- Extend and retract landing gears
- Open and close cargo doors
- Provide control for various utility applications

EMAs can be divided into two families:

- *Linear*: for electromechanical actuators, the rotary movement of the motor is converted into linear movement by means of gears such as ball, or roller systems if high loads must be transmitted.
 - Linear actuators can have the electric motor not integrated in the actuation system and transmit the motion with a gearbox, these actuators are called "*geared*", or they can have the electric motor integrated in the motion transmission structure, these are called "*Direct Drive*".
- *Rotative*: EMA rotary type the rotary movement of the electric motor is transformed with a gearbox.

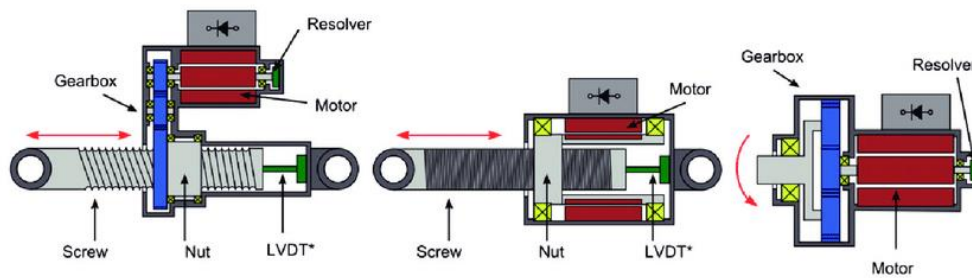


Figure 11: From left to right Geared EMA, Direct Drive EMA and Rotary EMA. LVDT: linear variable differential transformer.

Figure 11 shows the differences between the main three types of electromechanical actuators. In general, each electromechanical actuator consists of a mechanical drive unit, a power control system and a signal control system. a servomotor is required to be compact, with a high rotation speed and high reliability in the case of flight commands, servomotors of this type must have a high-power density. The motors used to drive the electromechanical actuators are:

- PMSM, permanent magnet synchronous motor.
- BLDC motor, Brushless Direct Current motor.
- Switched reluctance (SR) motor.

Gearboxes transform from high to low motor revolutions; according to the laws of mechanics, gearboxes transform low input torques to high output torques at low revolutions. Gearboxes represent a high proportion of the total mass of the electromechanical actuator, it is important that these components have a low mass. Electromechanical actuators all have a module that controls the power and derives the current to be supplied to the motor. CU uses voltage pulse amplitude modulation (PWM signal modulation). The position of the actuator is determined by a position sensor positioned on the output and another sensor is positioned on the motor rotor to monitor the currents passing through the stator phases. Temperature sensors are also fitted for flight controls for improved system safety.

Hydro-mechanical Actuators

Hydromechanical actuators were the first solutions adopted in aviation to enhance flight

controls. With the development of increasingly large, high-performance aircraft, aerodynamic compensations were insufficient to be safely managed by the pilot; the increasing size of aircraft also led to an increase in the loads transmitted to the control surfaces, so the drive system had to withstand increasingly high loads. The need to upgrade the flight controls was evident; the first solution is to use hydro-mechanical servomechanisms, the Figure 12 below shows a simplified diagram of how they work.

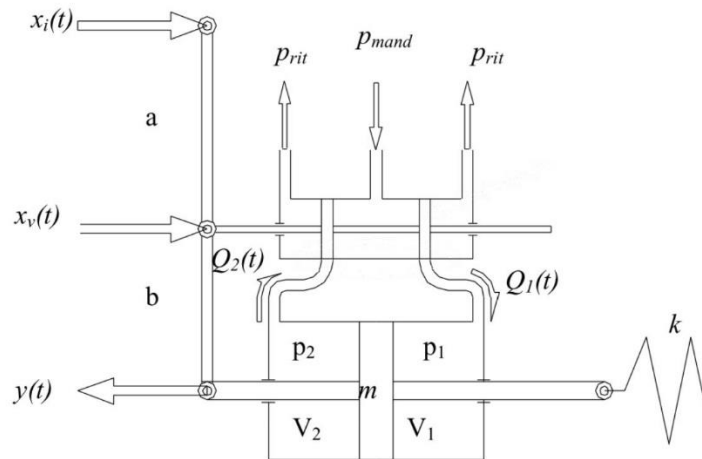


Figure 12: Hydro-mechanical actuation.

The pilot controls the activation of the command and moves horizontally by an amount of $x(t)$; the lever of length $a + b$ rotates around the lower end of b which is a point of instantaneous rotation, this movement leads to a displacement of the spool to the right by a quantity $x_v(t)$, the spool by moving makes hydraulic oil pass into chamber 1 of the actuator and makes hydraulic oil flow out of chamber 2 into the tank. The actuator with mass m then moves from the right to the left by an amount $y(t)$; spool closing is caused by the movement of the actuator; that rotating around the upper end of the lever, which is the center of rotation; the movement brings the spool back to the center position and stops the load actuation. Hydromechanical actuators have proved effective in controlling high loads, the hydraulic supply circuit allows greater flexibility in design and in particular it is possible to position the hydraulic pump away from the actuator to save space in the wing caisson, this is one of the main advantages of hydromechanical actuators, nowadays they are used in few applications, this type of solution being replaced by electro-hydraulic actuators.

Electro-hydraulic Actuators

One of the most widely used state-of-the-art solutions are electro-hydraulic actuators, which are used in flight controls and landing gear drive systems; this type of actuator is widely used for its high reliability and their precision of movement during their actuation.

Electro-hydraulic actuators are used in flight controls: the pilot using, for example, the stick generates an electrical signal which is transformed into mechanical movement through a valve and a hydraulic circuit. Figure 13 represents the block diagram of an electro-hydraulic actuator.

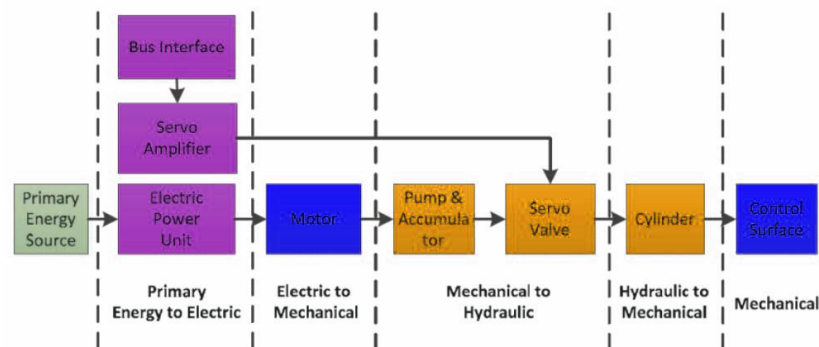


Figure 13: Block diagram of electrohydraulic actuator.

The pilot generates an electrical signal, the signal is compared with a position sensor and generates an error, the comparison is made by the control unit which evaluates the current position of the actuator via a position sensor or a speed sensor; using the error signal the control unit sends a proportional signal to the servo valve. The task of the servo valve is to convert an electrical signal into a hydraulic flow to move the actuator. There are many different types of servo valves on the market, but in general they always consist of two parts, firstly a motor and secondly a spool that determines the opening or closing of the circuit.

The electrical signal produced by the control unit flows into the windings of the electric motor and generates a magnetic field. The interaction between the magnetic field produced by the windings and the permanent magnet produces a rotation of the motor. The motor is connected to a flapper, during rotation the flapper is moved closer or further away from the nozzles. The displacement causes a pressure difference between the two nozzles. The Figure

14: Flapper-nozzle valve Figure 14 shows the displacement of the flapper.

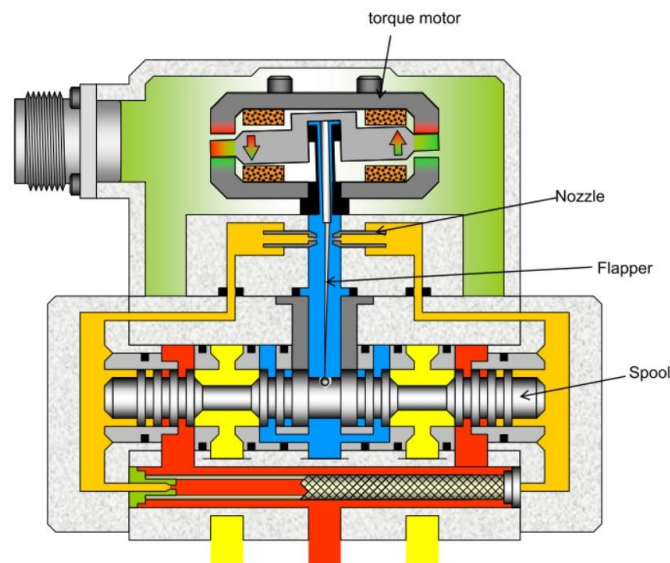


Figure 14: Flapper-nozzle valve

The difference in pressure at the ends of the nozzles is transmitted to the ends of the spool, which moves in the opposite direction to the flapper. Displacement of the spool returns the flapper to the central position. The movement of the spool produces the passage of fluid through the valve. Pressurized oil then passes through the openings in the valve and drives the actuator; the movement of the piston causes some oil to flow into the second chamber of the valve and back into the reservoir. In this condition the valve remains open and continues to actuate the hydraulic piston and the spool is not centrally positioned. When it is necessary to terminate the fluid passage, the motor is no longer powered, the valve is subject only to the force of the spring feedback; the flapper is close to a nozzle and this causes a pressure increase in the respective chamber. The wrong force in this situation is opposite to the force generated with the circuit activated and so the spool moves to the initial position where the oil passages are closed. The displacement of the spool also positions the flapper centrally, rebalancing the pressures on the two nozzles.

Flapper nozzle valves are the most common, but jet-pipe valves can also be found. Jet-pipe valves work in a similar way to flapper-nozzle valves. Instead of a flapper, a jet pipe is installed; the direction in which the oil flow is delivered determines the displacement of the spool. Figure 15 shows a simplified scheme of jet pipe valve.

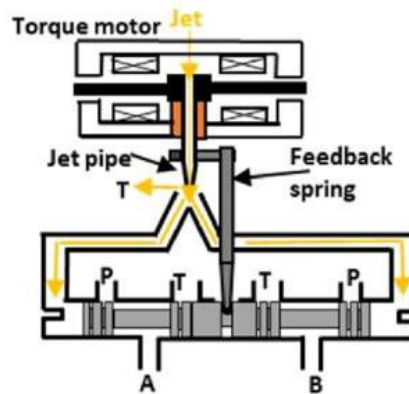


Figure 15: Jet-pipe valve.

Electric motors

The progress of technology has led to the realization of increasingly efficient electric motors, at the state of the art there are two major families of electric motors, which are classified according to the DC or AC power supply. DC motors can have commutators (brushes) or be homopolar, AC motors are divided into asynchronous motors and synchronous motors, in the figure below you can see the main subdivisions of electric motors.

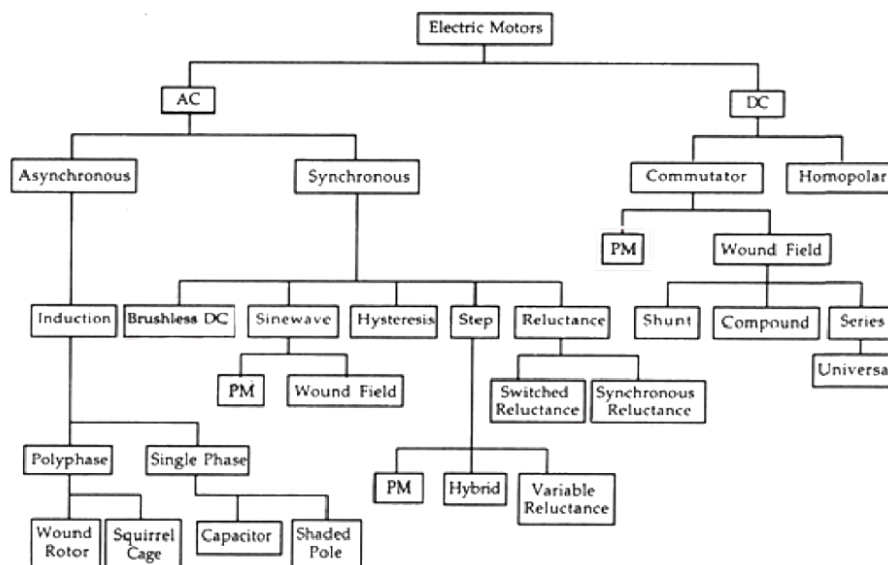


Figure 16: Electric motors classification.

Brushless motors are the most used motors in aeronautics because of their main property of not having brushes and therefore of not creating sparks. the choice of actuations through the absence of brushes is due to the high performance and in the control of the movement very precise.

To understand how a brushless motor works it is necessary to understand the physical laws that govern the motors and what interactions there are between the stator and the rotor.

Lorentz Law

Lorentz force is the force exerted on a charged particle q moving with a velocity v with respect to the reference system inside a magnetic field B .

$$F = q v \times B$$

Where the module of the force F is equal to:

$$F = qvB\sin(\theta)$$

With θ the angle between speed vector and the orientation of the magnetic field. To calculate the modulus of the Lorentz force exerted on a stretch of wire of length L and crossed by a current I immersed in a uniform field B , is necessary integrate the previous expression and obtain:

$$F_l = I B L$$

Using this principle, it is possible, by passing a current through an electric wire to obtain a force proportional to the current and the intensity of the magnetic field. The figure below shows a simplified diagram of the operation of a DC electric motor with brushes.

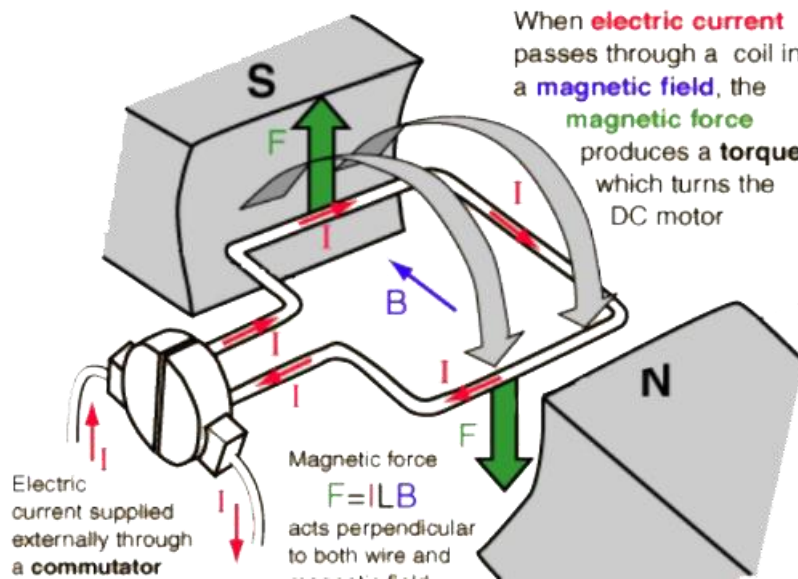


Figure 17: Scheme of a DC motor.

The Lorentz force creates a rotary movement in the electrical coils in which the current passes, for motors with brushes it is necessary to change the direction of passage of the current at each turn to be able to operate the motor in a direction of rotation.

Brush/Brushless motors

The biggest difference between a DC motor and brushless motor consists that in the latter the permanent magnets are on the rotor and the electrical windings are placed on the stator. Brushless motors have a very smooth operation, they are efficient and stable, thanks to encoders placed inside it is possible to control using a closed loop. The motor used in the development of this thesis is a sinusoidal three phase brushless motor. The operation of three phase motors is obtained by a commutation of the three phases at a precise frequency. Therefore, result a rotation of the electric field created by the windings that will rotate and the magnetic head present in the rotor tends to align. In order to obtain a correct commutation of currents is necessary to know at all times the position of the rotor.

The encoder is a very precise position sensor that can detect the position of the motor shaft along the revolution. The most common encoders are the Hall effect encoders which

measure the variation of the electric charge at the sides of a conductor.

Unlike DC motors, brushless motors have few phases, in general, three connected in a star. there are two families of brushless motors: trapezoidal and sinusoidal motors.

On the trapezoidal motors the magnetic flux that is concatenated with the windings of the stator is linear at times for high angles of rotation of the rotor, a consequence is that the counter electromotive force is constant at times.

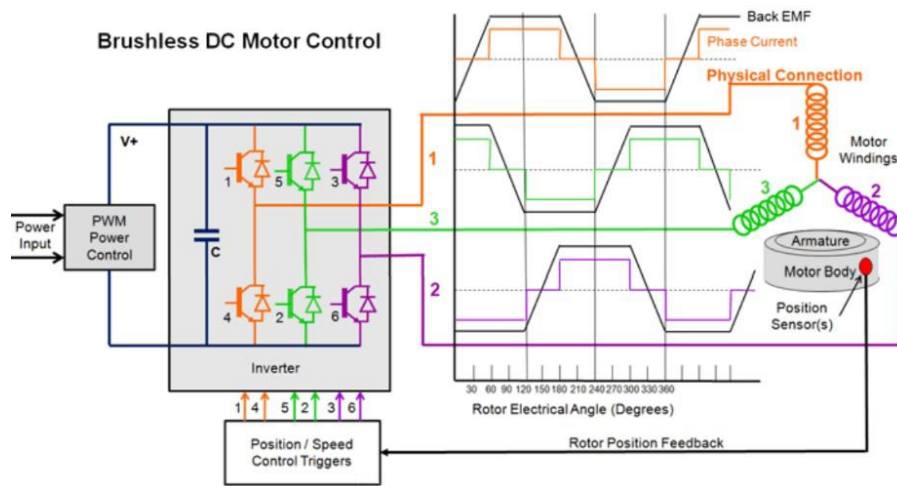


Figure 18: Trapezoidal control motor.

The sinusoidal brushless motors recreate the rotating field of Galileo Ferraris. The counter electromotive force (CEF) corresponding to a phase has a sinusoidal trend in time; for this reason, it is necessary to know precisely at each instant the position of the rotor in order to switch correctly the phases.

The position detector can also be used as a speed detector to control a speed in closed loop; to generate the currents in the star connected phases it is necessary to use power transistors by means of the pulse modulation technique (PWM).

The currents circulating in the motor phases are at a frequency imposed by the operating condition of the motor and are adapted moment by moment. The three currents are still sinusoidal functions, but of the motor position, and their amplitude is varied proportionally to vary the motor torque. At steady state, the shape of the three currents is sinusoidal as a function of time. whereas in trapezoidal motor control only two stator windings are active during a PWM cycle, in sinusoidal motor control all three stator windings are always active;

this leads to a more regular motion.

Operating sequences of the sinewave motor and the trapezoidal motor are similar, a trapezoidal drive sequence is shown below but it is the same. The phases are organized at 120° with respect to each other and are powered by an inverter which regulates the switching of the phases over time. the creation of a magnetic field due to the windings creates a phase shift with the magnetic field created by the permanent magnet present in the rotor; the rotor tends to align itself with the field created by the windings, this interaction produces a torque at the motor shaft. This process is carried out continuously by the inverter in order to rotate the motor shaft.

Planetary gearbox

Motion is generated by motors, which convert electrical energy into mechanical energy (in the case of motors with an electrical supply). The mechanical energy can be transmitted by means of gears, cardan joints, belts, chains, gears.

For the applications studied in this thesis, the electric motor generates a rotary motion applied to the shaft; for useful applications it is necessary to vary the number of shaft revolutions, then use gears to transmit the motion to the user and make the torque and number of revolutions just right for the user to operate correctly.

The following relationship relates the motor and user torques to the number of revolutions at the ends of a gearbox:

$$C_M \omega_M = C_U \omega_U$$

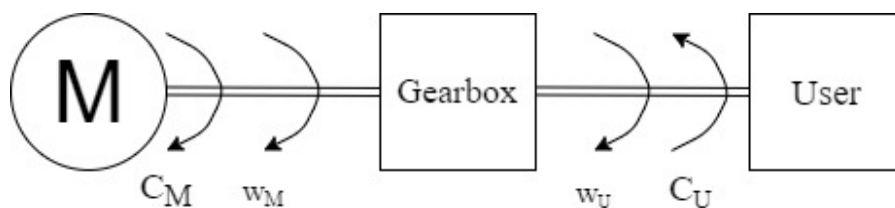


Figure 19: Motor-Gerabox-User diagram.

Through the above relationship, in general, it is better to have the motor with a high revs shaft and low torque for a cost-effective solution. The tool for transmitting and transforming motion are planetary gears. The main geometrical characteristics of gears are:

- *Upper and lower circumference*: these two values identify maximum tooth height and throat position; the height of the tooth is given by the difference between the upper and lower circumference.
- *Modulus*: represents the ratio of pitch to pi, then the pitch can be expressed using the teeth number and the primitive radius:

$$m = \frac{p}{\pi}$$

- *pitch*: this is defined as the distance between two successive tooth profiles. in the case of gearwheels, it is possible express the primitive circumference as the product of the pitch “p” and the teeth number “z”.

$$p = \frac{2 r \pi}{z}$$

Planetary gears consist of a series of wheels, the biggest difference between ordinary gears is that planetary gears have a series of fixed shafts and moving shafts. Sun gears are wheels that do not engage with each other and have a fixed axis, sun gears are generally applied as input and output of the planetary gear. Called Planetary gears are the wheels that rotate around the sun gear; planetary gears also rotate in the inner gear. Planetary shafts are supported by the carrier. The carrier rotates at the same speed as the planetaries, but around a fixed axis coinciding with the axis of the sun gear.

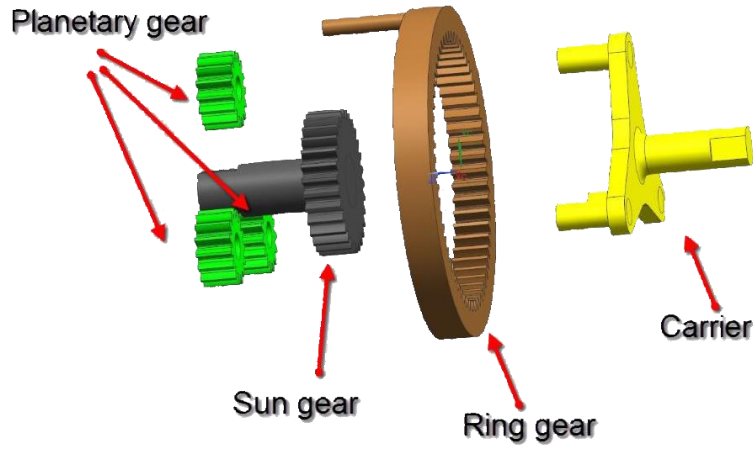


Figure 20: Detail of planetary gearbox.

The parameter characterizing the planetary gearing (in addition to the primitive radius, module and pitch of each individual wheel) establishes the relationships between the gears. The transmission ratio of the planetary gear is indicated by τ_w Willis formula:

$$\tau_w = \frac{\omega_{uot} - \Omega}{\omega_{in} - \Omega}$$

This formula represents the fundamental relationship in planetary gears; where Ω represents the angular velocity of the carrier. the value of the gear ratio can also be calculated as the ratio between the number of teeth between two wheels. The following figures show this calculation:

$$\begin{cases} \tau_{a,b} = \frac{\omega_b}{\omega_a} = -\frac{Z_a}{Z_b} \\ \tau_{b,c} = \frac{\omega_c}{\omega_b} = -\frac{Z_b}{Z_c} \end{cases}$$

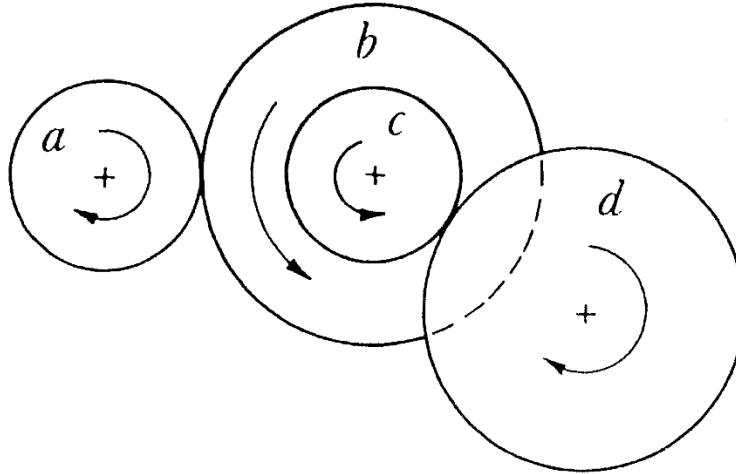


Figure 21: Rotating wheels.

Opposing load vs aiding load

It is important to underline an important aspect of efficiency for gearboxes; in fact, the efficiency varies in case where there is an opposing load placed on the user or if the load is in an aiding condition.

These two situations cause the efficiency to vary, the efficiency of gears is higher with an opposing load while it is lower in the case of an aiding load. The demonstration is shown next.

To carry out a demonstration, it is necessary to introduce some concepts of mechanics applied to machines, in particular some concepts relating to the transmission of motion.

It consider a simple body for transmitting motion: a lever that functions as a reducer.

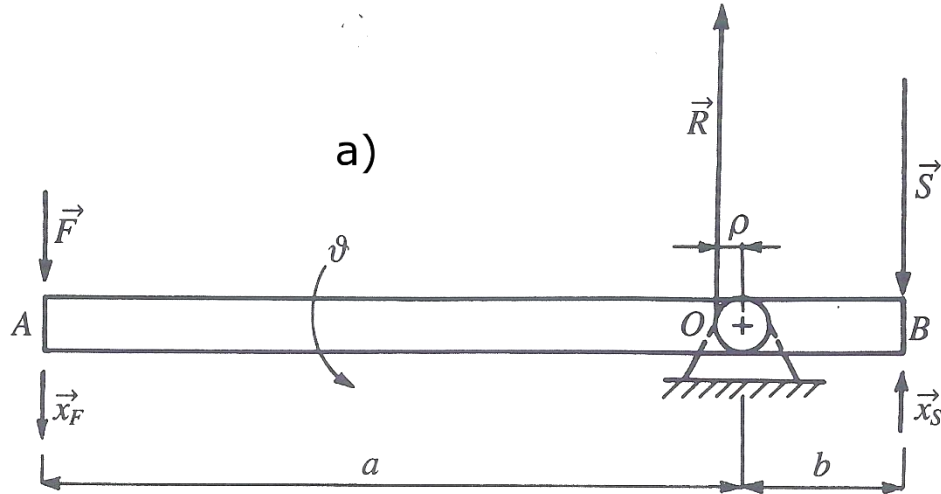


Figure 22: Simplified scheme of a reducer a).

The lever is fixed at point "O" which allows only rotation; the radius of the circle of friction called ρ is known.

Two forces are applied to the lever, a driving force F at the extremity A, and a load on the extremity B with the letter S. Therefore, the rotation is counterclockwise in the case of "figure a)". The downward displacement of the extremity A is called \vec{x}_F and is given by the expression:

$$\vec{x}_F = a \cdot \vartheta$$

While the displacement of extreme B is given by the expression:

$$\vec{x}_S = b \cdot \vartheta$$

From the work equation we can deduce that the force \vec{F} performs positive work, while the load performs negative work. The work is expressed as:

$$W_F = Fa\vartheta \qquad W_S = Sb\vartheta$$

Efficiency is the ratio between two works:

$$\eta = \frac{Sb\vartheta}{Fa\vartheta} = \frac{Sb}{Fa}$$

Now the steady state conditions are analyzed, it is possible to write an equilibrium equation of momentum with respect to the point of limit reaction (point of application of force R in Figure 22 a)):

$$F(a - \rho) - S(b + \rho) = 0$$

Using the efficiency expression written previously:

$$\eta = \frac{1 - \frac{\rho}{a}}{1 + \frac{\rho}{b}}$$

Now consider a second situation, similar to the previous case, but the rotation is clockwise.

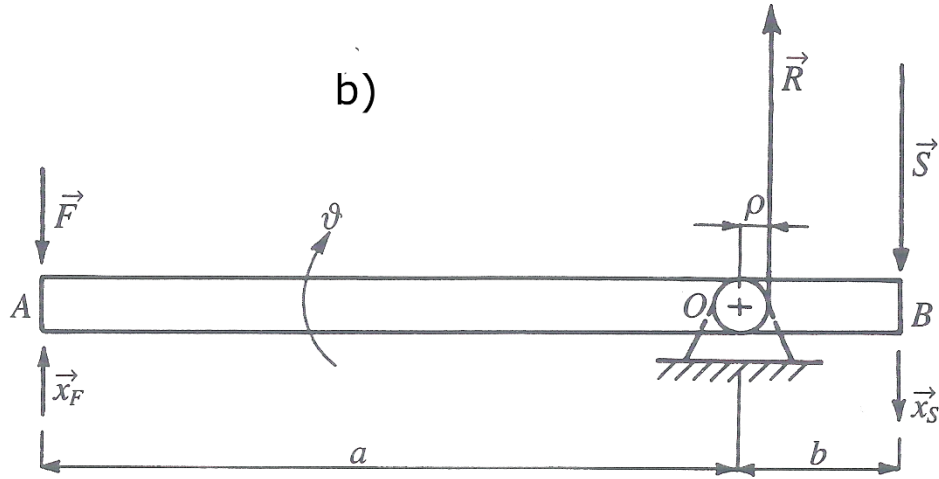


Figure 23: Simplified scheme of a reducer b).

The displacement of extremity B is concordant with the direction of application of load S; therefore displacement x_S is greater than displacement x_F ; in this case the power flow goes from point B to the extreme A; now we calculate the efficiency in this condition, the expression of the efficiency is:

$$\eta' = \frac{F a}{S b}$$

The relationship between the force vector F and the load vector S is obtained as shown above, in this case the constraint reaction will be closer to point B. If we face the momentum equation with respect to the point of application of R it obtain:

$$F(a + \rho) - S(b - \rho) = 0$$

It is now possible to derive the efficiency in this new condition:

$$\eta' = \frac{1 - \frac{\rho}{b}}{1 + \frac{\rho}{a}}$$

If the two efficiency expressions found (in the gearbox condition and in the multiplier condition) are compared, it can be shown that they have two different values. Let us assume the following values:

- $a = 1$ meters;
- $b = 0.1$ meters;
- $\rho = 0.01$ meters;

The final values of η and η' are:

$$\eta = 0.9000 \quad \text{and} \quad \eta' = 0.8911$$

These results show that the variation in efficiency depends on the friction radius ρ .

This demonstration leads to the conclusion that:

1. The efficiency of a gearbox decreases with angular speed ratio, the efficiency of a gearbox decreases with increasing angular speed ratio; it can be concluded that a gearbox with a transmission ratio of 1/60 has a worse efficiency than a gearbox with a transmission ratio of 1/10; a gearbox with a transmission ratio of 10 has a better efficiency than a gearbox with a ratio of 50.
2. Speed reducer is the best choice than multiplier for the same gearbox.

Backlash

Mathematical models simulate with reasonable accuracy the linear behavior of a real phenomenon. The study of natural phenomena under transient or boundary conditions has led to the conclusion that almost all systems possess non-linearity; for this reason, it is important to be able to study this phenomenon and find algorithms that simulate these behaviors. The most common form of non-linearity is friction behavior. This phenomenon is assumed to be linear and proportional to speed in the case of viscous friction between two surfaces; in the case where the speed is zero, there should be no friction. In the latter case,

there is actually an amount of static friction (called Coulomb friction). The transition from the condition of static friction to the condition of viscous friction is not a linear phenomena. The Figure 24 shows how the friction coefficient varies as the sliding speed increases, it is called “*Stribeck Curve*”.

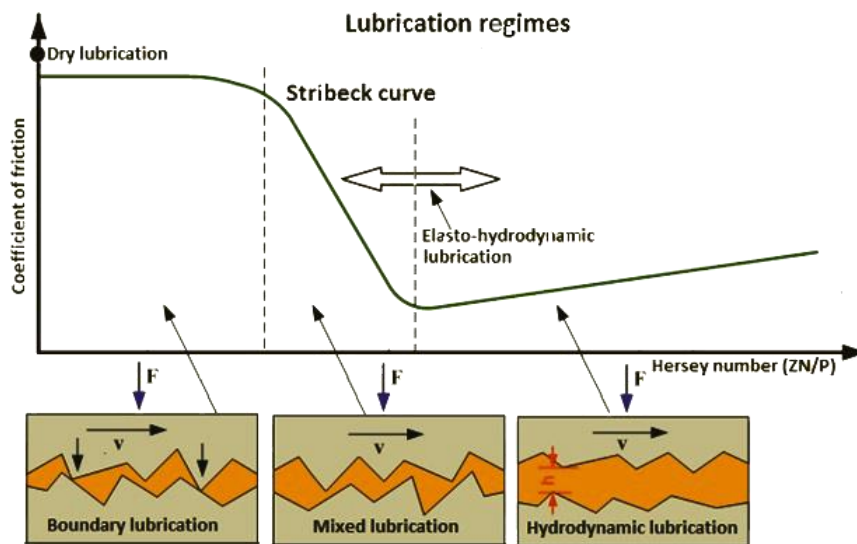


Figure 24: Lubrification regimes.

In mechanics, a common non-linearity when studying gearboxes is gear backlash. This phenomenon can be caused by incorrect assembly between two gears (radial distance between the two-wheel centers), which may cause gear backlash between the teeth. A very common situation in which gear backlash is experienced is when the input motion to the gearbox reverses direction, in which case there is a relatively small transient where the input gear is rotating while the output gear is stopped, this is due to the entire gearbox system having to recover gear backlash on all wheels between input and output.

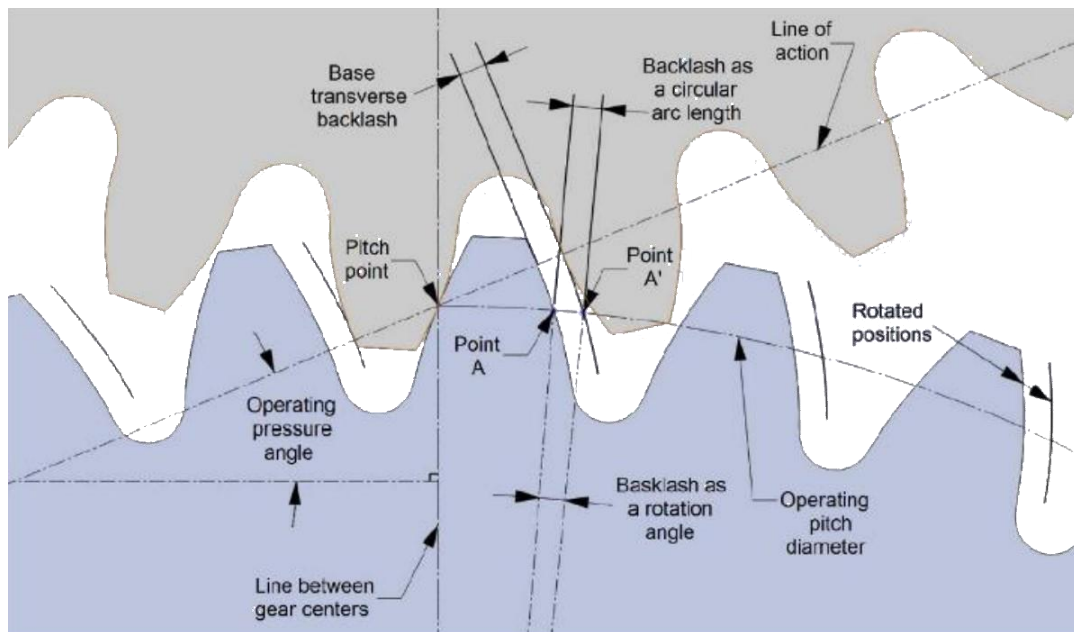


Figure 25: Gear backlash definition.

During the construction of gearboxes, it is possible for defects to occur, such as cutting errors, shaping, installation techniques, tooth thickness errors, profile, lead.

One of the parameters that most affects the performance of gearboxes is the gear backlash. This parameter is assessed when the whole gearbox is assembled. There are three methods for assessing this parameter:

- Mechanical
- Electrical: through resolvers.
- Optical: through scopes.

Commonly it is measured along the line of action or along the pitch of gears.

The phenomenon of gear backlash contains two factors: a variable part and a constant part, these two phenomena are still under study. In the following paragraphs we present the mathematical calculation to obtain the gear backlash as the distance between the gear axes varies.

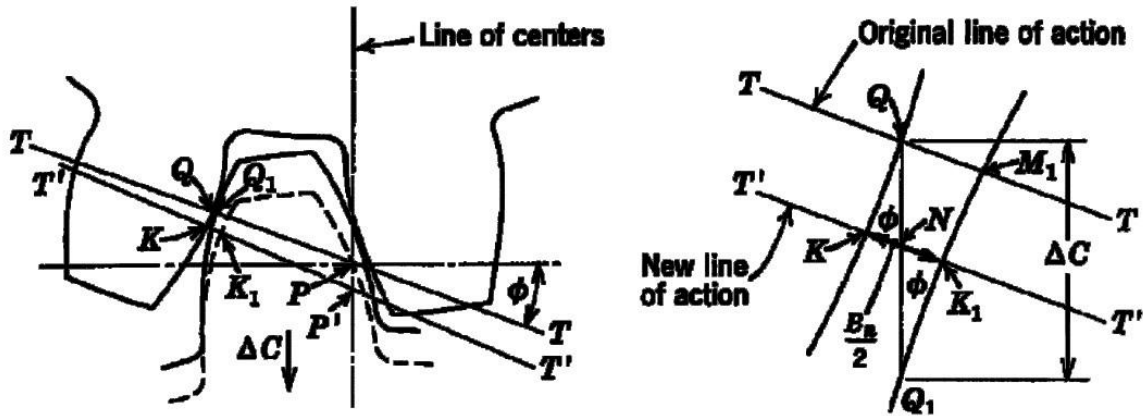


Figure 26: "Backlash caused by center distance change: left: mated teeth before and after increase of center distance, Right: enlarge view of profiles and backlash ".

It is possible to express the slope of the line of action as the product of the forces exchanged at the tooth contact point as the ratio of the normal to the parallel components (K and Q respectively) and Φ is the pressure angle.

$$\frac{KK_1}{QQ_1} = \sin \Phi$$

Where the dot product KK_1 is the normal backlash measured on the action line; this product is equal to $KK_1 = \frac{B_n}{2}$ and the product $QQ_1 = \Delta C$.

Making some substitutions:

$$\frac{B_n}{2} = \Delta C \sin \Phi$$

Gear backlash commonly refers to the primitive circle of the gear wheel, through the formula just derived it is possible to refer it to the primitive circle and considering to open the profile of teeth on top of each other, the total gear backlash results to be:

$$B_n = 2 \Delta C \sin \Phi$$

Using trigonometry to refer gear backlash B to the primitive radius of the gear wheel, so the formula results:

$$B = 2 \Delta C \tan \Phi$$

This formula is applied to evaluate gear backlash on test bench.

Within the Simulink model there is a hysteresis block which simulates the backlash. The backlash is applied in the PID subsystem, in particular after speed integration. The backlash block is placed on the angular position branch expressed in radians, this position is referred to the fast shaft (motor's shaft).

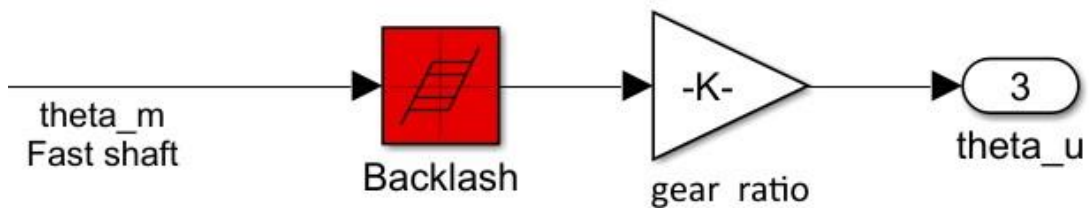


Figure 27: Backlash block.

The backlash values are all experimentally calculated but an initial backlash value is added to all data. The added value is given by measurements on the test bench and takes into account all the backlash in the planetary gear and assembly defects. The value detected by the encoder (with no backlash) positioned on the last stage of the planetary gear is: 0,365568 degrees.

Test bench overview

Introduction

This test bench has the purpose of evaluating various operating conditions of electrical motor and the gearbox.

The main goal of a test bench realization is to validate the computer models. Through the MatLab/Simulink model it is possible to evaluate nominal conditions and some failure conditions, for example coil malfunction or a backlash condition.

The construction of the test bench took a long time. First of all, it has been realized a CAD model of the main parts of the test bench: supports, gearbox, encoder, bearings. This is a fundamental phase to evaluate the dimensions of each part and therefore proceed to a correct realization of the test bench.

The Figure 28 below shows a gearbox assembly.

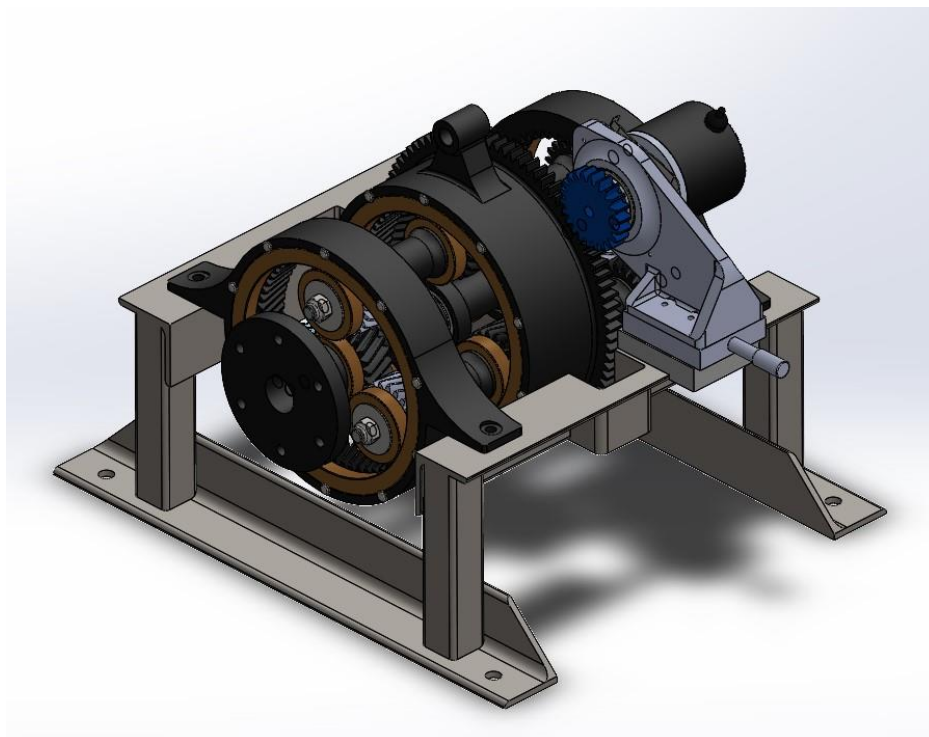


Figure 28: Gearbox - encoder assembly.

The model realization it was useful to evaluate the final size of gearbox and its supports. Another important issue is the evaluation of inertia of planetary gearbox, through the Solidworks modeling is possible precisely evaluate the inertia of gears.

Test bench has been modified several times up to the state of the art in which the electric motor is connected by means an elastic coupling to the planetary gearbox, the latter is associated, with the its slow shaft, to an encoder which is connected to the control unit, this represent the outer closed loop. The motor is also connected to a brake through a chain, Control Unit, PLC and computers are related each other with ethernet cables and switch port. The Arduino board controls the actuator and the brake through a load cell, and board is connected to PC.

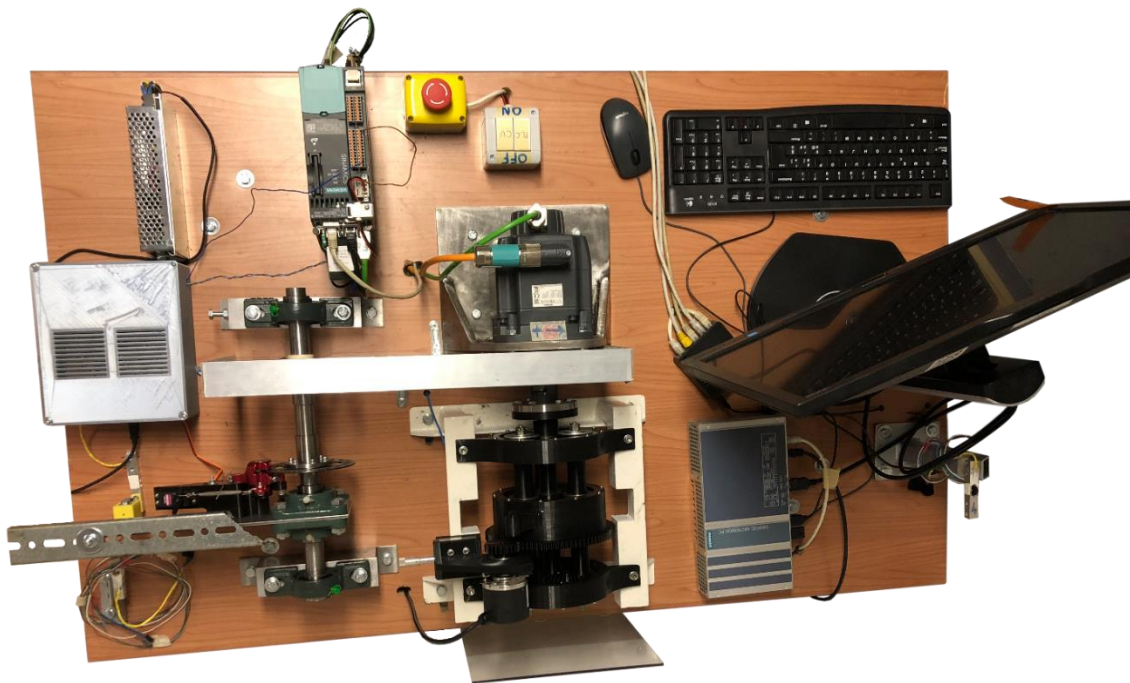


Figure 29: Test bench.

To make clear the connection of all items here, below, is represented a simplified scheme of test bench.

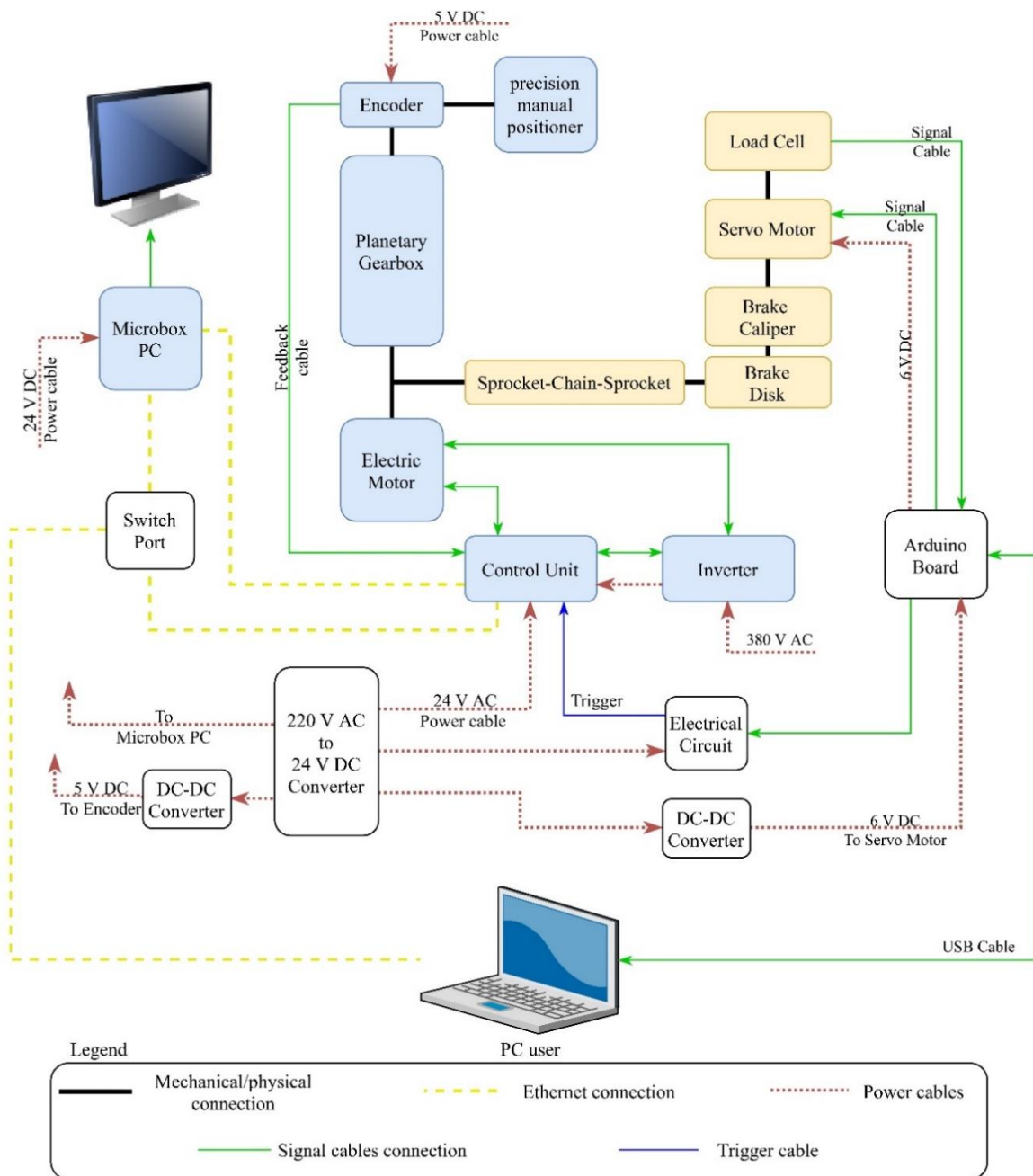


Figure 30: Test bench diagram connections.

In the Figure 30 there are all principal part that made up test bench. Between electric motor and planetary gearbox there is a mechanical connection with an elastic joint, another mechanical connection with motor and brake through chain system. The Encoder is mounted at the end of planetary gearbox on a gear wheel, this feedback system (Encoder and gear wheel) are not fixed, the whole system can be moved radially in order to vary the distance between the axis of the user and the axis of rotation of the Encoder; this way is adopted to varying gear backlash on each test; the loadcell measure the load applied on the motor.

Arduino board compute the actuation of the brake caliper in order to maintain a constant load value. Microbox, Inverter and control unit provide of running and control electric motor. The ethernet connections are used to give the desired commands to the motor and to carry out the necessary measurements; Trigger signal is used to the synchronization between load cell values and encoder time values through an electrical circuit. Finally, there are power cables which carry the necessary current to power correctly the users.

SINAMICS Control Unit - CU310-2



Figure 31: Control Unit.

Control Unit provides the regulation and function drive handling, this unit is powered by 24 V DC and controls the electric motor with a close loop via the “DRIVE CliQ” interface.

CU310-2 PN (PROFINET) is connected via ethernet cables with directly Microbox PC and with the switch port. Using the X22 serial interface (RS232) inputs port is possible to realize the encoder close loop; it is important to underline that the power supply of the encoder is not carried out by the control unit but is achieved through a stepdown that switches 24 V to 5 Volt. This solution is adopted for the correct functioning of the encoder.

Using the port “X120 fail-safe digital inputs/temperature sensor input” in particular the third

port is possible receive and record and input gave by Arduino board; this inputs during postprocessing phases is used to synchronized load cell and test bench data.

The Control Unit is equipped with a card slot dedicated to the insertion of a CompactFlash Card, and an area in which the Basic Operator Panel, the BOP20, is inserted.

The control unit is mounted on the top of inverter.

Simatic Microbox PC



Figure 32: Microbox PC with on the top the license key.

SIMATIC IPC427E Microbox PC provides to human interface and data handling, this unit is supplies by 24 V DC. This Microbox PC provides to control operations with the ability to implement control methods created using codes like C or C++, or using a software controller / WinCC RT Advanced. It also ensures the ability to collect, view and process data. It also allows the use of integrated and parameterizable monitoring functions (program execution / watchdog timer, processor and board temperatures).

For this thesis Microbox PC is used to control a sinusoidal position command to evaluate gear backlash.

MAIN FEATURES	
Processor and Fieldbus	Intel® Core™ i3-6102E Processor
Solid State memory	128 GB SATA
Memory	16 GB DDR4-SDRAM SODIMM
Operating system	Windows Embedded Standard 7 SP1, 64 bit
Graphic	HD graphic
Installation	Installation on DIN rail, wall mounting or vertical mountig
Power supply	24 V DC (-20%/+20%) max. 4 A
OTHER FEATURES	
Graphics	2 x DisplayPort DPP
USB Ports	4x USB V3.0 (high current)
Ethernet ports	3x Gbit Ethernet
Keyboard, mouse	external USB port

SINAMICS PM 240-2 Power module



Figure 33: Inverter PM 240-2.

This module works like an inverter and supply the motor windings using the law given by control unit.

This module is located under the control unit and is connected through the PM-IF interface, inverter module is powered by 380 V AC voltage source the main features are shows below:

Blocksize PM240-2	
<i>Rated Data</i>	
<i>Input</i>	
<i>Number of phases</i>	3 AC
<i>Line Voltage</i>	380 - 480 V $\pm 10\%$
<i>Line frequency</i>	47 - 63 Hz
<i>Rated current (LO)</i>	39.90 A
<i>Rated current (HO)</i>	36.00 A
<i>Output</i>	
<i>Number of phases</i>	3 AC
<i>Rated voltage</i>	400 V
<i>Rated current (LO)</i>	32.00 A
<i>Rated current (HO)</i>	26.00 A
<i>Max. output current</i>	52.00 A
<i>Rated power IEC 400V (LO)</i>	15.00 kW
<i>Rated power NEC 480V (LO)</i>	20.00 hp
<i>Rated power IEC 400V (HO)</i>	11.00 kW
<i>Rated power NEC 480V (HO)</i>	15.00 hp
<i>Pulse frequency</i>	4 kHz
<i>Output frequency for vector control</i>	0 - 200 Hz
<i>Output frequency for V/f control</i>	0 - 550 Hz

Figure 34: Inverter data.

Motor

One of the central parts of the bench tester is the electric motor. Test bench is armd with a sinusoidal permanent magnet electric motor produced by Siemens, the model is: "SIMOTICS S synchronous motor 1FK7060-2AC711CG0", in the figure below a picture of it.



Figure 35: SIMOTICS S synchronous motor.

This electric motor has no brushes, it is called brushless motor and it is powered by a 380V AC inverter it is used for industrial applications. The electric motor is connected with a planetary gear through an elastic coupling. Load torques are applied directly to the shaft through a chain sprocket motion transmission system.

Motor inputs are made through "*DRIVE CliQ signal cable*" this cable provides the necessary signals to the motor to switch phases, feeds the phases and provides feedback signals.

SIMOTICS S synchronous motor 1FK7060-2AC71-1CG0	
<i>Engineering Data</i>	
<i>Rated speed (100 K)</i>	2000 rpm
<i>Number of poles</i>	8
<i>Rated torque (100 K)</i>	5.3 Nm
<i>Rated current</i>	3.0 A
<i>Static torque (60 K)</i>	5.00 Nm
<i>Static torque (100 K)</i>	6.0 Nm
<i>Stall current (60 K)</i>	2.55 A
<i>Stall current (100 K)</i>	3.15 A
<i>Moment of inertia</i>	7.700 kgcm ²
<i>Efficiency</i>	90.00%
<i>Physical constants</i>	
<i>Torque constant</i>	1.1 Nm/A
<i>Voltage constant at 20° C</i>	121.0 V/1000*min-1
<i>Winding resistance at 20° C</i>	2.75 Ω
<i>Rotating field inductance</i>	30.5 mH
<i>Electrical time constant</i>	11.10 ms
<i>Mechanical time constant</i>	1.75 ms
<i>Thermal time constant</i>	30 min
<i>Shaft torsional stiffness</i>	40500 Nm/rad
<i>Net weight of the motor</i>	7.1 kg
<i>Mechanical Data</i>	
<i>Motor type</i>	Permanent-magnet synchronous motor
<i>Shaft height</i>	63
<i>Cooling</i>	Natural cooling
<i>Radial runout tolerance</i>	0.040 mm
<i>Concentricity tolerance</i>	0.10 mm
<i>Axial runout tolerance</i>	0.10 mm
<i>Vibration severity grade</i>	Grade A
<i>Connector size</i>	1
<i>Degree of protection</i>	IP64
<i>Temperature monitoring</i>	Pt1000 temperature sensor
<i>Electrical connectors</i>	Connectors for signals and power
<i>Holding brake</i>	without holding brake
<i>Shaft extension</i>	Plain shaft
<i>Encoder system</i>	Encoder AM24DQI: absolute encoder 24 bits (resolution 16777216, encoder-internal 2048 S/R) + 12 bits multi-turn (traversing range 4096 revolutions)
<i>Optimum Operating point</i>	
<i>Optimum Speed</i>	2000 rpm
<i>Optimum Power</i>	1.1 kW
<i>Limiting Data</i>	
<i>Max permissible speed (mech.)</i>	7200 rpm
<i>Max permissible speed (inverter)</i>	4750 rpm
<i>Maximum torque</i>	18.0 Nm
<i>Maximum current</i>	10.7 A

Encoder

A toothed wheel with 22 teeth is mounted on the last stage of the planetary gear; encoder is placed on the shaft of the toothed wheel. The encoder model used is produced by “*Italsensor company*” of the type "*TSW581HS.M2.5000.5.V.K4.B127.PL10.PP2-5*". This model of encoder is of incremental type. Incremental type encoders measure increments with respect to a position, regardless of the direction of rotation. Encoders of this type are useful for detecting shaft position, speed, or accelerations. This encoder has three communication channels (channels A, B, Z); channels A and B produce a square wave that is 90° out of phase with respect to each other, reading channels A and B at the same time makes it possible to obtain variations in the position of the shaft and also the direction of rotation; the Z channel is used if you want to have a measure of the number of revolutions.

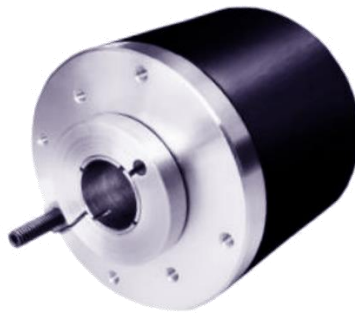


Figure 36: Encoder.

The main features of the encoder are shown below.

ENCODER SPECIFICATIONS	
Model	TSW581 (bidirectional + index)
Assembly	M2 (with spring type M2)
Pulse rate	5000
Power supply	5 (+ 5 V \pm 5%)
Output frequency	V (from 0 a - up to 300 kHz)
Protection degree	K4 (IP 64(EN60529))
Shaft diameter	B127 (12.7 mm)
Electrical connections	PL10 (radial cable gland with cable 1 ÷ 6 m long)
Output circuits	PP2-5 (Push-Pull 5 V output only)
Resolution	10000 ppr
Power supply	5 V, 5÷28 V, 11÷30 V
Output frequency	up to 300 kHz
Synchronous index output	on A default, B-A+B optional
Supply current without load	150 mA max
Operating temperature	-10°C ÷ +70 °C
Protection	short circuit protection, no limit duration (only output LD2 and PP2); against inversion of polarity (except 5 V, 5/28 V)

Brake module

The braking system of the bench test provides the resistant torque applied to the motor shaft.

The braking system consists of:

- Motion transmission system consisting of sprocket, chain, pinion.
- Braking system through a disc and a caliper.
- Actuation system consisting of a servomotor driven by an Arduino board.
- Load cell.

The torque transmission shaft is positioned parallel to the motor shaft and is supported by bearings at the ends. The brake disc has holes to improve heat dissipation that accumulated during braking; the servomotor is connected to the brake caliper via an adjustable shaft to compensate for brake pad deterioration. This System is equipped with a load cell to measure the braking force and to close the servomotor control loop. The control of the brake is made up through an Arduino board that given as input the braking torque value to be maintained a consequently the board actuates brake to follow the value provided.

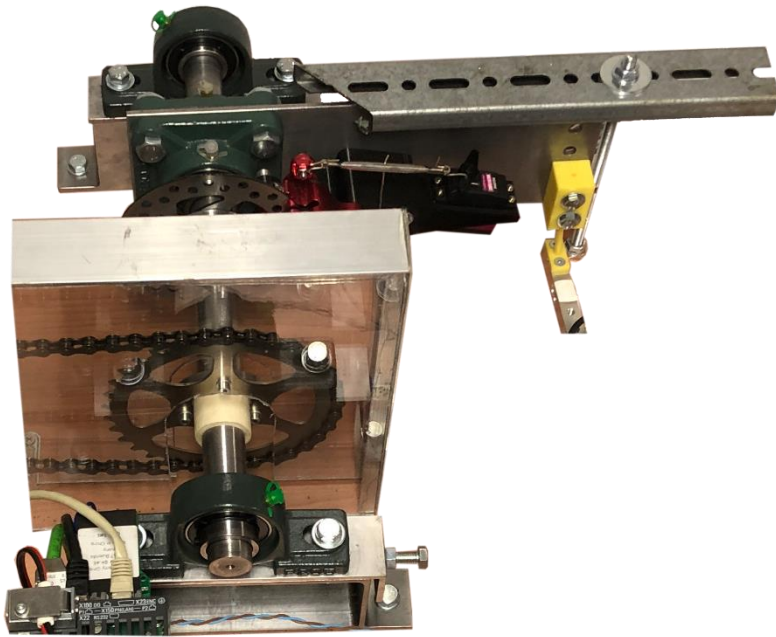


Figure 37: Braking module.

Trigger System

The trigger system has the function of changing state in a precise instant, when the Arduino board begins starts reading the load cell values sends a signal (the trigger) to the control unit which is recorded by the starter. To obtain a signal that can be read by the Control unit, it is necessary that this has a high enough voltage, it is necessary to use a transistor system to switch the voltage from a low to a high state.

A transistor system with MosFet and Bjt was created in order to control a high voltage with a small voltage coming from the Arduino. The wiring diagram is as follows:

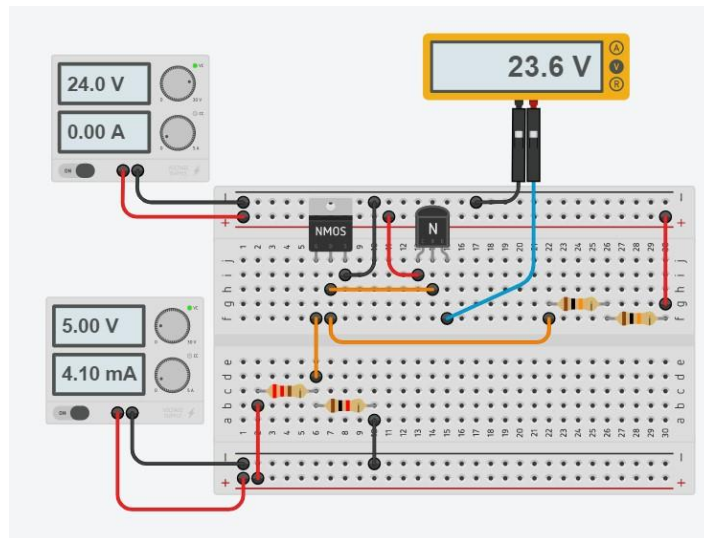


Figure 38: Electrical scheme for trigger switching.

In the Figure 39: Configuration of transistors. it is represented the scheme realized:

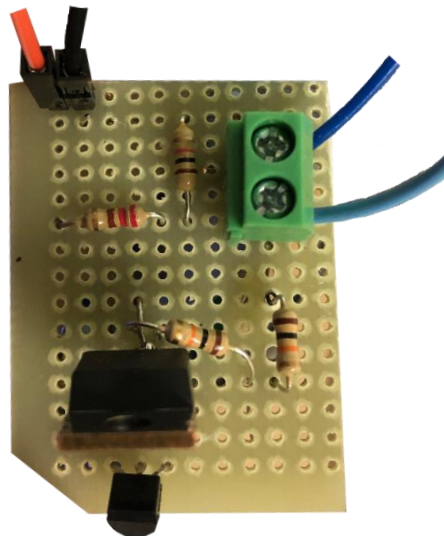


Figure 39: Configuration of transistors.

Quick guideline for test bench

Introduction

Inside this chapter it's shows a short guideline to approach and start correctly the test bench.

The purpose of the guide is to give the user the knowledge to use the bench test at its best and avoid some commons mistake.

This test bench is composed by: Motor, planetary gearbox, encoder, Microbox PC, Control Unit, Inverter, brake system, Arduino board.

In this first release test bench is drive by “*SIMOTICS synchronous motor 1FK7060-2AC71*” which is controlled by a control unit coupled with an Inverter. Signals are manage by PLC which is simulated inside Microbox PC: “*SIMATIC IPC427E Microbox PC*”; synchronous motor is connected to planetary gearbox and then to an optical incremantal encoder (“*TSW581HS.M2.5000.5.V.K4.B127.PL10.PP2-5*”); the latter is assemble with a precision manual positioner to set gear backlash. In order to apply a braking force, there are a brake drive by an “*Arduino*”. The trigger signal is generated when the Arduino board become to read the load cell values to synchronized *Starter* Software values with Loadcell values. Trigger cable is blue and it go from Control Unit to Arduino box.

Figure 40 below show how test bench is connected.

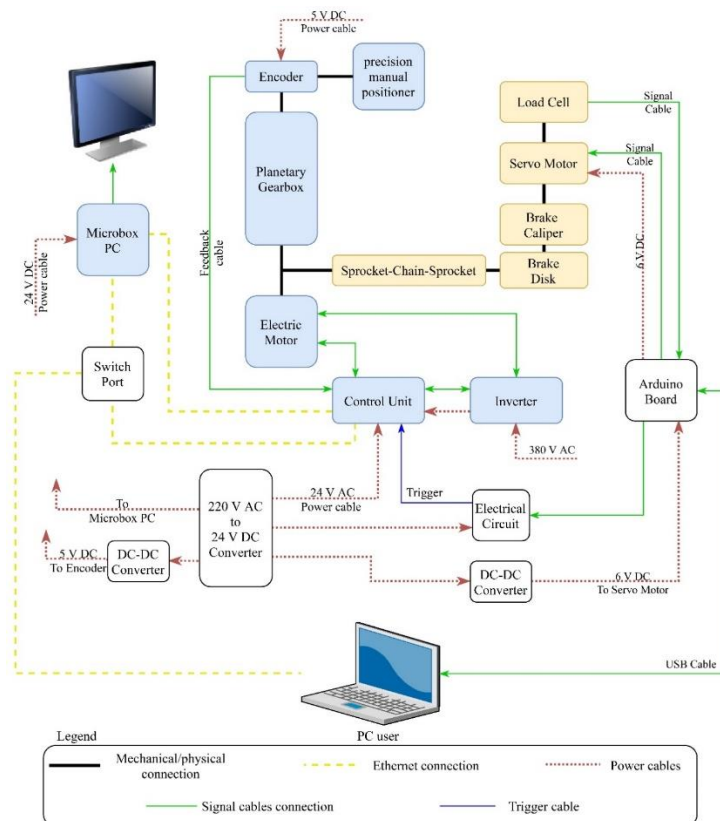

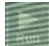


Figure 40: Test bench connections.


Turn on test bench and hardware connections

- Connect power supplies: brown wire to 380 V AC and black wire to 220 V AC.
- Turn on the screen.
- Turn on alimentation of Control unit.
- Turn on alimentation Microbox PC and then switch on the button on its case.
- Windows embedded is now starting.
- Pull up the emergency button to alimentation for the electric motor.
- If required any password digit:1234
- Double click on desktop icon: “Software PLC_I”.
- Press button  to initialize the communication with the control unit.
- Press “Run” button  to enable the communication between PLC and Control Unit.
- Connect Ethernet cable to PC.
- To enable web server communication using: IP 192.168.0.2
- Connect the USB Arduino Cable to PC.

Warning: Switch on the button on the right side of the gray box that containing Arduino board

Best PC setting: is preferable use two PC, one with installed “*Starter*” to record motor and encoder data; another PC is required to control motor through Web server and record load cell values with MatLab; both PCs should be connected via Ethernet cable.

Software connection: Starter to test bench

- Download “*Starter*” software from this link:
<https://support.industry.siemens.com/cs/document/26233208/sinamics-micromaster-starter?dti=0&lc=en-AE>
- Open Starter.
- To import projects, paste project folder in the following:
C:\Programmi\SIEMENS\Step7\S7Proj
- Click on  to connect computer to the test bench.
- Click on “*play*” to record data.

How to set and start test bench using Web server

- Using the current browser digit IP: 192.168.0.2
- The figure below represents the principal screen



Figure 41: Web server main screen.

- Press on “ENTER” to enter in the control panel.
- The Figure 42 shows the main menu, through this window it is possible to access all the settings for starting up the test bench.

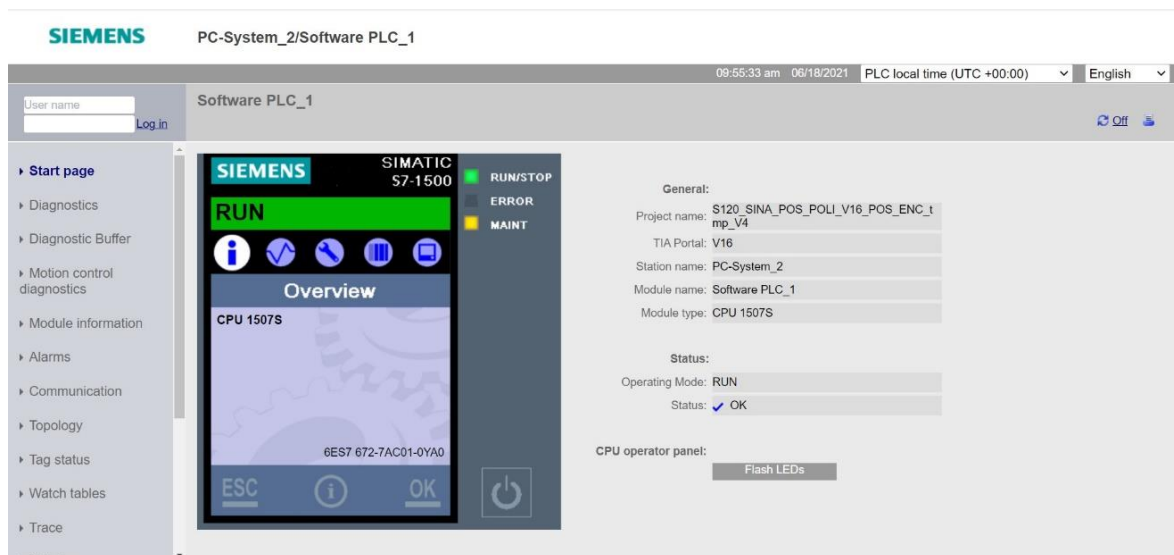


Figure 42: Main menu.

How to set commands

From the menu that shows in the Figure 42 on the left, click on "User-defined pages" and then on the link: "Homepage of the application command_block_r2020a_V2". then click on "WorkspaceParams". The following window will appear; it will be possible to set the parameters of the commands and then click on "Submit" button.

- Sinusiodal signal:
 - Amplitudes and biases are used in degrees;
 - Frequencies are used in Hertz.

Parameter	Value	Action
ChpTg	0.5	Submit
RampG	0.0	Submit
RampSlope	1.0	Submit
RampTime	1.0	Submit
SinAmp	6.0	Submit
SinBias	10.0	Submit
SinFrq	0.2	Submit
StepFin	0.0	Submit
StepIni	0.0	Submit
StepTime	0.0	Submit
com		Submit

Exit Reload

Figure 43: Set commands window.

How to enable commands

From the main menu (Figure 42), click on the item "User-defined pages" and then on the link: "Homepage of the application command_block_r2020a_V2". Then click on the item "Params". The following window will appear; it will be possible to enable the commands using zero as a non-enabled command, and 1 as an enabled command. Through this window it is possible to provide more commands at the same time.

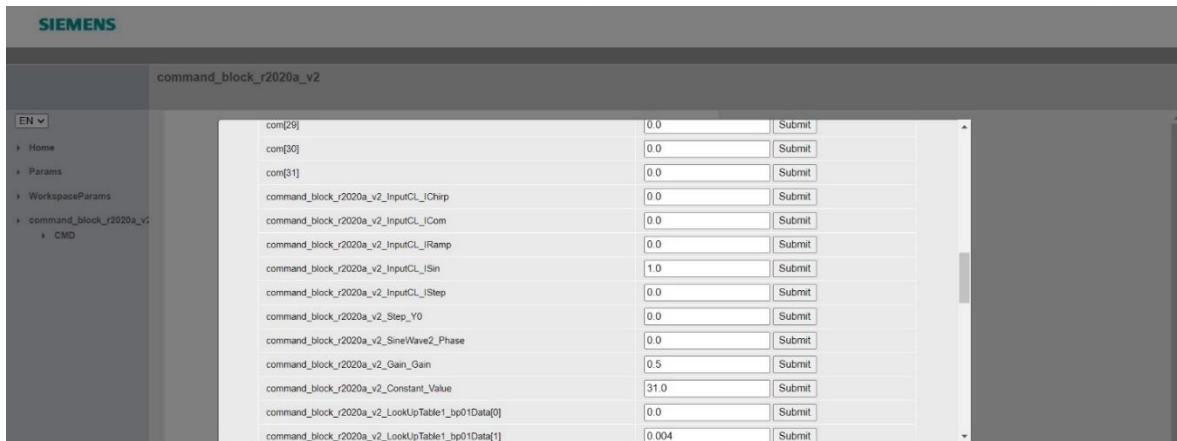


Figure 44: Enable command window.

How to start running test bench

Select “*watch tables*” from the main menu on the left, and using this screen is possible to run the motor.

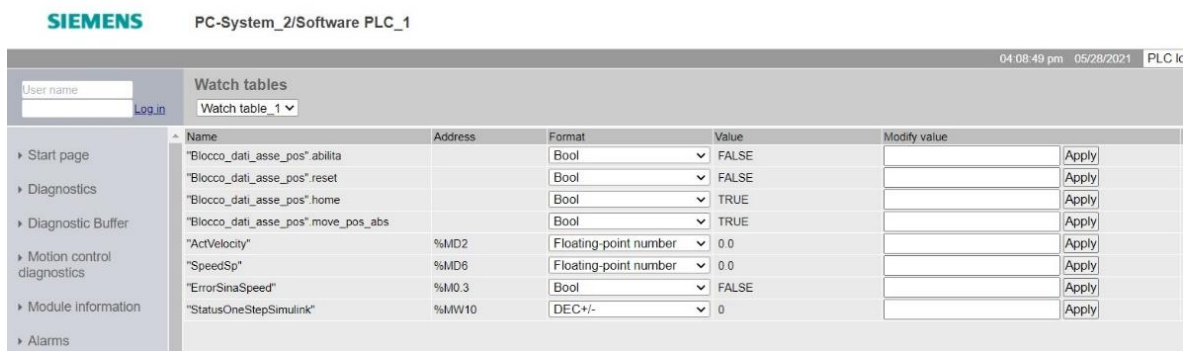






Figure 45: Start and Stop window.

- Set to TRUE and then to FALSE “*Blocco_dati_asse_pos*”.*reset*; this command detects input state changes.
- Set to TRUE “*Blocco_dati_asse_pos*”.*abilita*.
- Set to TRUE and then to FALSE “*Blocco_dati_asse_pos*”.*home*; this command detects input state changes.
- Set to TRUE “*Blocco_dati_asse_pos*”.*move_pos_abs* to run the command, that is previously generated.
- To stop engine set to FALSE “*Blocco_dati_asse_pos*”.*move_pos_abs*.

How to shut down test bench

- Save and close STARTER projects and web server pages.
- disconnect ethernet cables USB cables from PCs.
- Press emergency button to disable motor supply
- Through the test bench desktop press Stop button  and then press  to confirm the action.
- Press quit button  and confirm the action with  and wait until the PLC shut down.
- Turn off windows.
- Turn off PLC with the button on its case.
- Turn off Control Unit alimentation.
- Turn off PLC alimentation.
- Turn off the power strip.

HF model of electromechanics actuator

The purpose of the realization of high-fidelity (HF) models is to obtain a model sufficiently similar to reality and which can simulate the operating conditions of the test bench. An high-fidelity model also has the task of simulating the main system failure conditions. In the developed system, a particular wear condition of mechanical components is studied which leads to a gear backlash between the gears. Using MatLab/Simulink modeling the model was realized. This model simulates the behavior of a primary or secondary flight control; the response time of the model is between primary and secondary flight controls. Another important issue of realization of that model is that the model can evaluate other operative condition and its possible to apply this model to other areas, like electrical actuation for CNC machine.

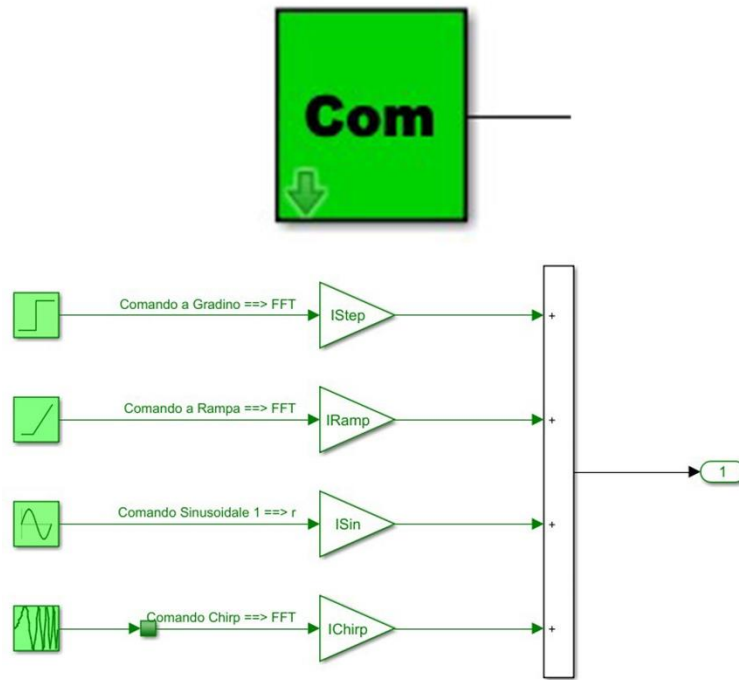


Figure 47: Command block.

Load generation – Load Cell values fitting

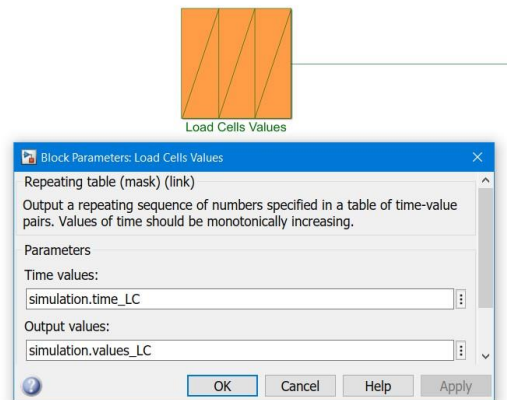


Figure 48: Load Cells values input block.

The block that provides the load values to the model is realized with a "Repeating sequence" block that given the time values and load cell values provides the model with the load value at the required time. If the load cell values do not have the same sample time as the HF

model then the repeating sequence block uses a linear fitting between the previous and the next value.

The time and load cell values are provided by the MaTlab script and Arduino board.

Control electronics (PID)

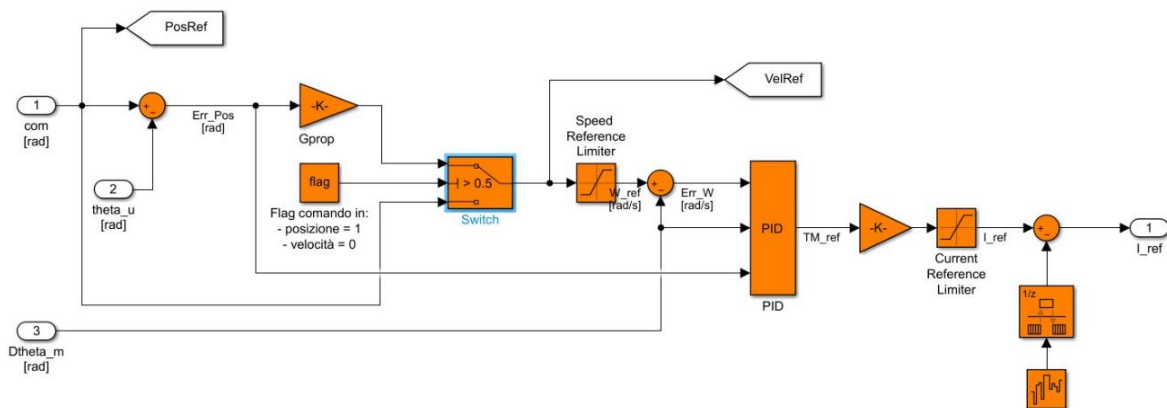


Figure 49: "Control Electronics (PID) subsystem."

Within Control electronics PID the command position value and the motor speed are provided as input. The former is compared with the position of the user, these two commands are provided in slow shaft and the unit of measurements are radians. Error generated is multiplied by the proportional gain and become an speed error and then pass through Switch block. The role of the "Switch" block is if the command is given on radian/sec; switch port bypass the error position. The position error is controlled by a saturation block to avoid values that could damage the motor; the speed saturation value has been set equal to the value present in the control unit of the test bench. After, the speed error enters in PID subsystem.

Figure 50: PID subsystem. Figure 50 shows in detail how PID is made.

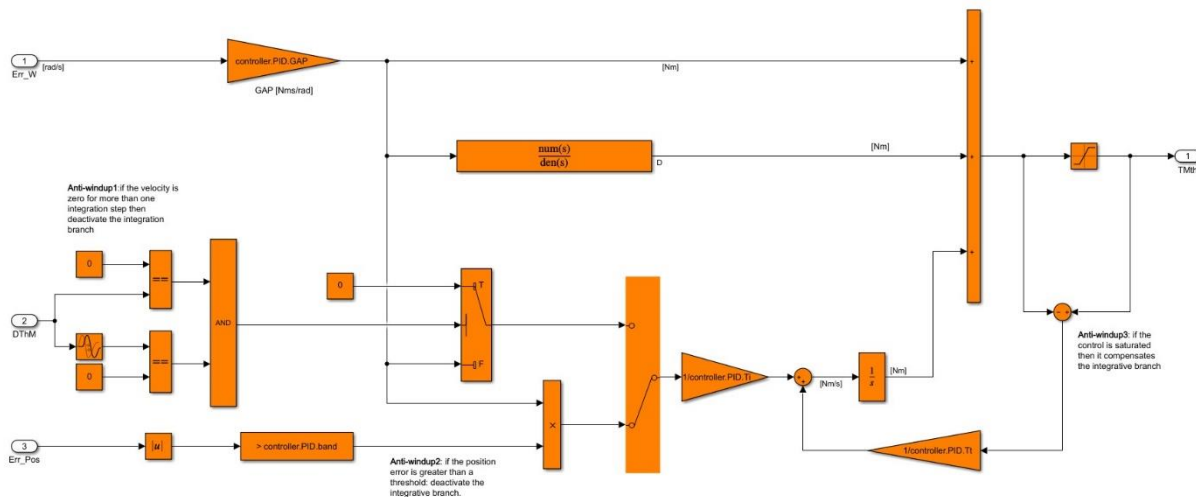


Figure 50: PID subsystem.

This subsystem receives as input a speed error expressed in radiant/second, angular motor speed and position error.

The design of a PID (Proportional-Integrative-Derivative) controller uses an active PD controller and then an active PI controller and adding or modifying poles or zeros in the s-plane; the s-plane is the plane where vector quantities of complex numbers are located; on the ordinate axis the complex part is represented while on the X-axis the real part is represented.

PI controllers are ideal controllers that use the "*ideal integral compensation*" technique; this technique involves inserting a pole into the origin of plane s and increasing the order of the system and reducing the steady-state error.

PD controllers are used to improve the transient response of a system; this controller is implemented through an error-based signal (proportional) and a signal based on the derivative of the error. PD design is implement by adding derivative control to the poles and zeros of the system to obtain acceptable transient response. [1]

Proportional branch

The proportional branch is defined by a multiplication of the error signal. the proportional part of the PID is used to amplify the signal and be able to control it.



Figure 51: Proportional gain.

Integrative branch

The steady-state error performance can be handled using integrative control.

The integrative branch multiplies the error signal for a gain ($\frac{1}{\text{controller.PID.Ti}}$) and then provides integration of the value. It is important to model this branch correctly in order to avoid the windup phenomenon.

The windup phenomenon is typical of digital PIDs: in case of very high tracking errors the integration block reacts with an intense action proportional to the error until it reaches the physical saturation value. During the saturation of the signal by the integrator, the error signal is continued to integrate and a residual error is created, due to the difference between the saturation level and the actual value of the error, this leads to overload the integrator; when the input signal goes out of saturation line the integrator continues to integrate with an error accumulated in previous integration steps. This fact lead the signal unstable e more difficult to control. To remedy this problem there are technological solutions, anti-windup techniques:

- *Anti-windup1*: This system allows to verify that if the speed is equal to zero for more than one integration step then the integrator is disabled to avoid excessive error accumulation. The implementation logic is carried out with Boolean blocks that compare the angular velocity value of the motor at the current integration step and the angular velocity at the previous integration step. This control includes the possibility of a end-stop insertion or the presence of static friction.
- *Anti-windup2*: This protection acts on the error position, if it is lower than a value then the integrator block is disconnected. This control handles friction effects that could cause the system stop on undesidered position.
- *Anti-windup3*: is used to compensate when the command is saturated. The compensation is done by comparing the value of the saturated torque command with the unsaturated torque command, if the sum between the two signals command is not

on saturation, instead, if the sum between the two signals is different from zero then the value is used to compensate and reduce the contribution of the block integrator.

Derivative branch

Derivative control is used to control the response of a system during transient. the transfer function that defines the derivative controller is as follows:

$$G(s) = \frac{T_d s}{\frac{T_d}{N} s + 1}$$

Assuming a characteristic time of $T_d = 0,01 \text{ sec}$ and $N = 1000$, it is possible to plot the root locus of the transfer function:

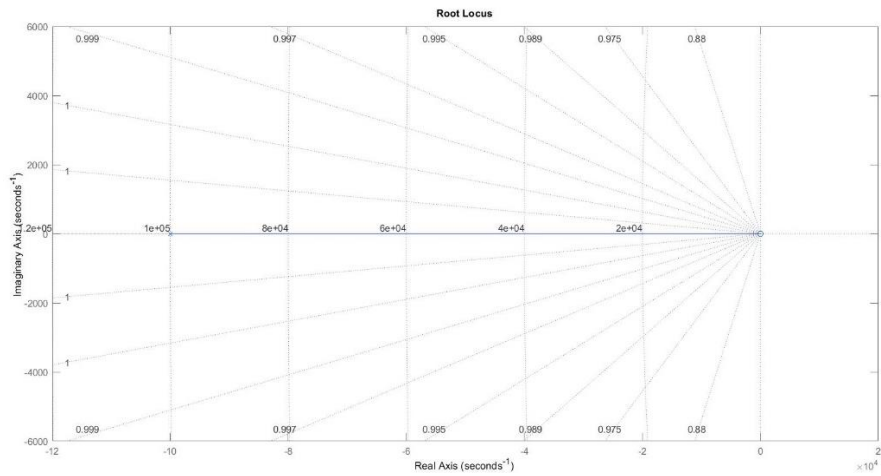


Figure 52: Root locus transfer function.

Inverter Model

This subsystem has its input the command current (“ I_{ref} ”) and the electrical angular

position of the motor's shaft and has in feedback the currents which pass in each single phase (" I_A , I_B , I_C "). this block returns $A1$, $A2$, $A3$.

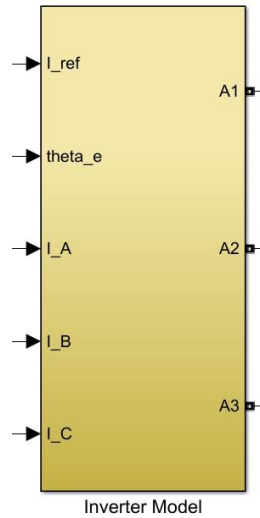


Figure 53: Inverter Inputs and Outputs.

The figure below shows how inverter model is composed, is clear to distinguish three main blocks:

- Evaluation of phase currents.
- Hysteresis PWM.
- 3-phase bridge.

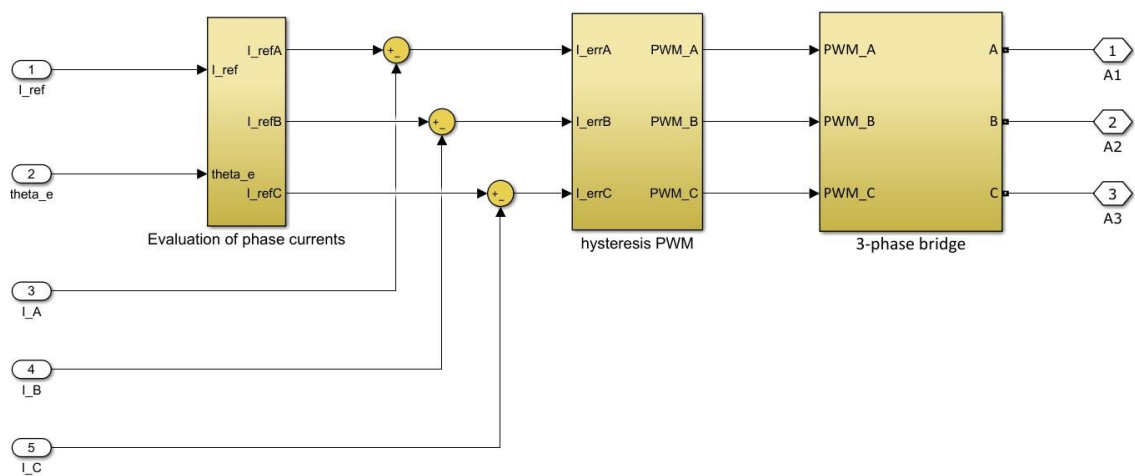


Figure 54: Inverter model subsystem.

Evaluation of phase currents

First is necessary understand how much current pass through each phase this evaluation is drive by Clarke-Park's reverse transformation. This transformation allows to obtain three-phase reference current (" I_{refa} , I_{refb} , I_{refc} ").

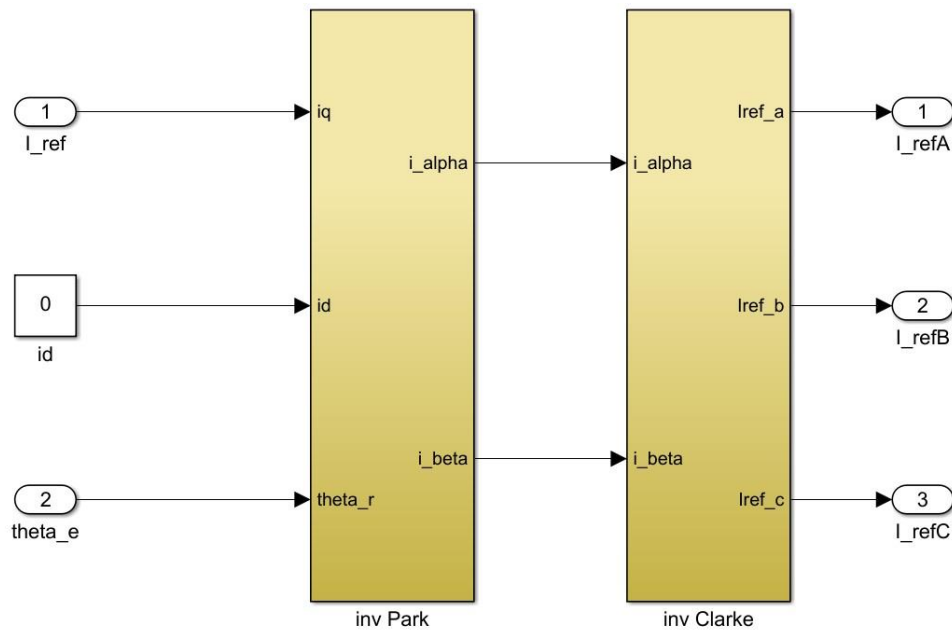


Figure 55: Reverse Park-Clarke transformation.

A short demonstration is listed, as below:

With the first matrix (Park matrix) it obtain a change of coordinates, passing from a quadrature current I_q and a direct current I_d and then pass to a Cartesian reference system with on axes Alpha and Beta, the two axes are axes united to the stator and therefore integral to the phases and rotate the reference system integral to the rotor of an angle theta and in a way that it is a quadrature with the magnetic field created by the stator and it obtain the two commanded currents that are the magnetic field components along beta and along alpha, then is used the Clarke projection that takes in input the two commanded currents that are the magnetic field components along the reference axes Alpha and Beta to go to transform these two components and provides in output the current components facing the windings, in the

case of the bench test the three windings equally spaced components a, b, c are rotated with respect to each other of 120° in this section we have decomposed only the commanded current and transformed in order to have all the current 90° in advance.

Hysteresis PWM

At this point is required to give an error input, to do this, the reference currents are compared with currents given by BLDC electromagnetic model to obtain a simple feedback control.

The errors generated are manipulated by three hysteresis blocks.

These blocks reproduce three PI (one for each phase) located inside the inverter. These PI has short response time, its magnitude is about milliseconds, they are very fast to follow motor's characteristic time.

To simplify control, it was introduced hysteresis block. The hysteresis control is implemented by switching the output signal on / off and inserting a dead band, in conclusion output signals are:

- The same: if the signal is small enough to remain inside the dead band, the output is the same of the previous integration step.
- 1: if the signal is higher than the upper threshold
- 0: if the signal is lower than lower threshold.

The hysteresis block generates a square wave in high frequency this wave is the PWM, those signals are used to active or deactivate the inverter, signal depend by the value of the real current value and the command currents

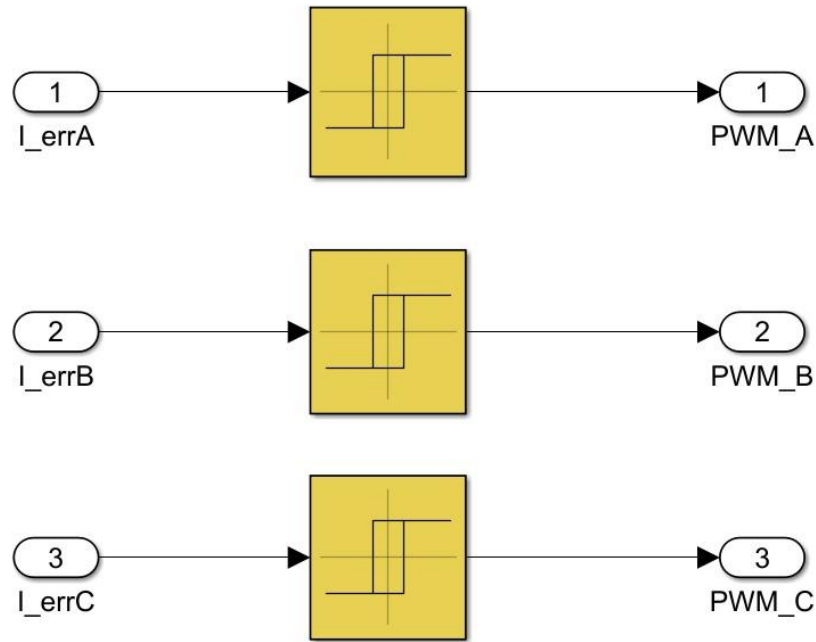


Figure 56: Hysteresis subsystem.

PWM technology

This technology as known as Pulse Width Modulation and transform logical inputs made of 1 and 0 on variable output value between minimum alimentation value and maximum alimentation value. Typically high value switch on the alimentation and zero value switch off the alimentation; the realization of this technique is carried out through a variation of the relationship between the duration of the impulse and its period, this variation is called “Duty Cycle”, the figure below shows how it is possible to obtain a variable voltage value between 0 and 5 Volt.

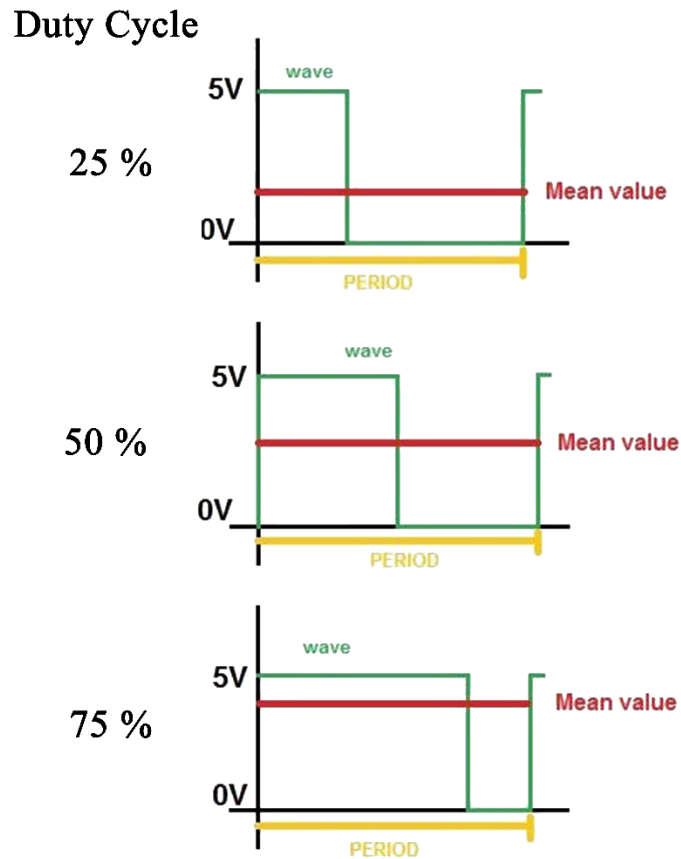


Figure 57: Duty cycles examples.

Using an on / off input where when the system is on it supplies the maximum output voltage and when the system is off it supplies zero voltage. It is possible to work on how long the system stays on and how long the system stays off and consequently the output regulation between the maximum of duty cycle and the minimum.

3-phase bridge

Three signals coming from Hysteresis block are converted into Boolean values to being processed by Simscape block. In the figure show below it is possible notice that are some negation blocks “NOT”; these blocks are applied to avoid grounding the power supply when signals go in Simscape block and cause short circuit situation. Alimentation is provided by “DC Voltage Source”, in this study the voltage is set on 380 Volt Direct Current.

Three signal and its negation are now vectorized and send to Simscape block called “Universal bridge” through g port; This latter block uses PWM signals and alimentation

source solve 3 equation to obtain three voltages called A, B, C that are used for commend electromagnetic model.

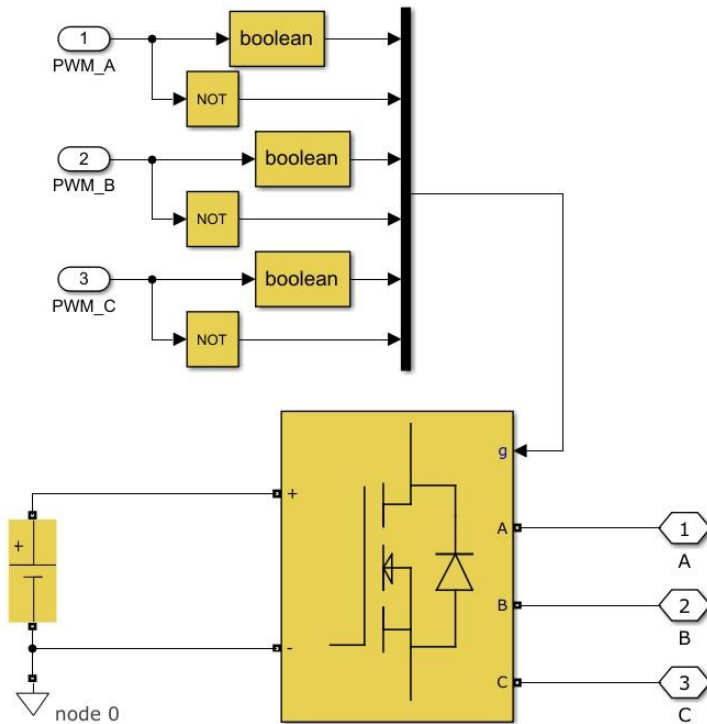


Figure 58: 3-Phase bridge.

The effective current swing inside the bandwidth almost $\pm 0,5$ Ampere around the value of command current. These oscillations are caused by the control using hysteresis; the effective current fluctuates inside the bandwidth with a triangular wave.

Electromagnetic model

“Electromagnetic model” subsystem represented the model of the motor, and three inputs from the inverter represented in this case a not a functional connection (for the simulation) but represented a real connection between inverter and motor.

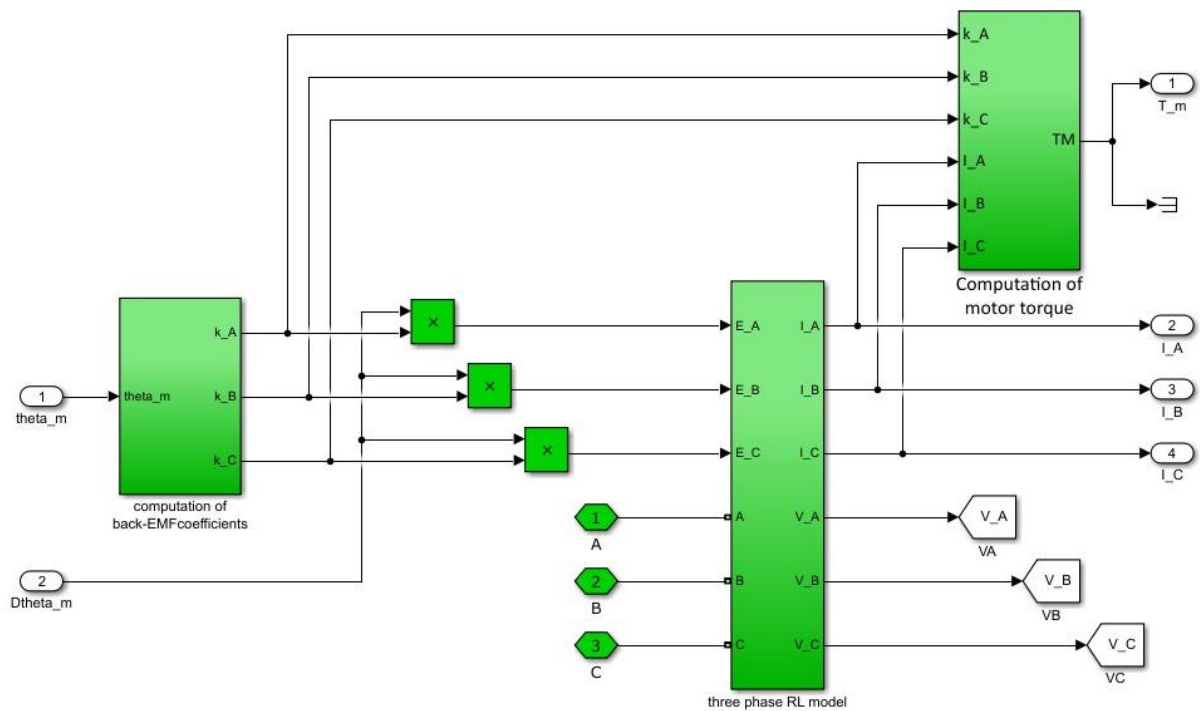


Figure 59: BLDC Electromagnetic model subsystem.

Electromagnetic subsystem is composed by three principal systems:

- Computation of back-EMF coefficients
- Three phase RL model
- Computation of motor torque

And receives on input the angular position and the speed of the rotor.

Computation of back-EMF coefficients

This block compute instantaneous counter electromotive force coefficients for each phase; mechanical angular position of the rotor is an input of this computation.

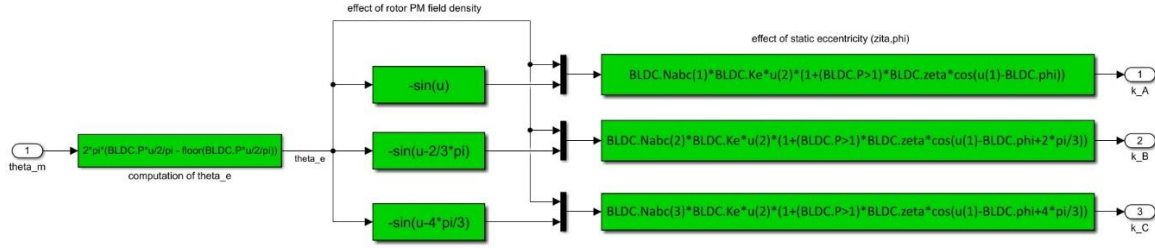


Figure 60: Computation of back-EMF subsystem.

First is useful transform the mechanical position ϑ_m to electric position, considering it has $P = 4$ polar pairs, with the relationship:

$$\vartheta_e = 2 \cdot \pi \left(\left(\frac{P \cdot \vartheta_m}{2 \cdot \pi} \right) - fl \left(\frac{P \cdot \vartheta_m}{2 \cdot \pi} \right) \right)$$

Through this expedient is possible obtain the electrical position, in the figure below is show how varies the electrical angular position every rotor complete rotation.

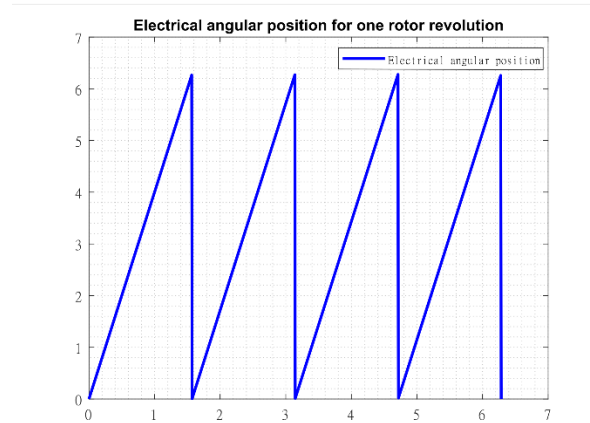


Figure 61: Electrical angular position.

The electrical position obtained is used to calculate the counter electromotive force for each phase. For synchronous brushless motor the counter electromotive coefficient force has a sinusoidal trend.

For one phase permanent magnet motor, the counter electromotive force (CEF) assume a

$$K_{fcm}^{(i)} = N_i K_e^{(i)} f(\vartheta_e) \cdot \left(1 + \zeta \cos \left(\vartheta_e - \varphi + \frac{2(i-1)}{3} \pi \right) \right)$$

$$K_{f_{cem}}^{(i)} = N_i K_e^{(i)} f(\vartheta_e) \cdot \left(1 + \zeta \cos \left(\vartheta_e - \varphi + \frac{2(i-1)}{3} \pi \right) \right)$$

Through this mathematical formula is possible add some fault inside coils. N_i represents the active i-th coil fraction; $K_e^{(i)} f(\vartheta_e)$ is the calculus of the nominal counter electromotive force without any fault injection, the other part of the equation is used to taking into account the static eccentricity and the static eccentricity phase, these two parameters are ζ and φ respectively; during ideal operation of the electric motor these two parameters are set to zero. During life cycle there is the possibility that air gap between stator and rotor becomes unequal, due to any misalignment, broadly there is two main type of eccentricity:

- *Static eccentricity*
the rotor axis does not rotate on the same axis as the stator, this type of eccentricity requires the mass distribution to be symmetrical with respect to the rotor axis, static eccentricity often depend by bearing construction or wear phenomena.

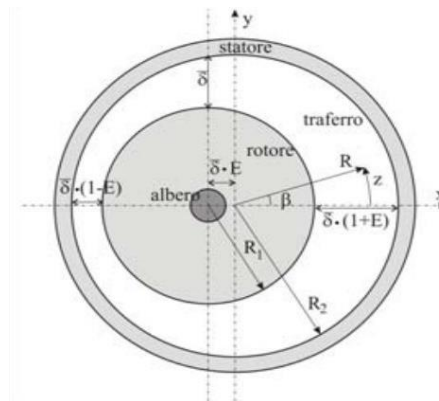


Figure 62: Static rotor eccentricity.

- *Dynamic eccentricity*

The rotor and the stator axes rotate on the same axis, the mass distribution is not symmetrical with the rotor rotation axis. The figure below explains the behavior of dynamic eccentricity.

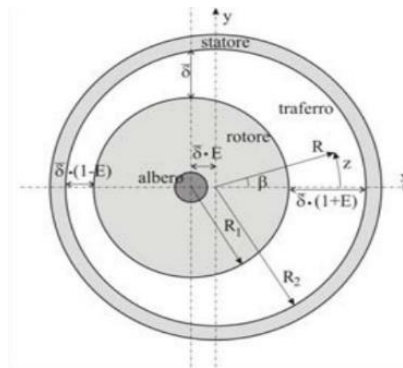


Figure 63: Dynamic rotor eccentricity.

The MatLab/Simulink model implement the static eccentricity; the implementation is realized by two parameters shown above, where ζ represent the modulus and φ the phase of static eccentricity, the effect of this eccentricity is that: if the air gap has a variation in thickness this phenomena produces a variation of magnetic reluctance (air gap thickness increase produce the permeability increase); during electric revolution the magnetic field lines are facilitated to pass through the areas where the air gap is more thin, the formula remodel the counter electromotive parameter on the electric revolution to implement the static eccentricity.

Three phase RL model

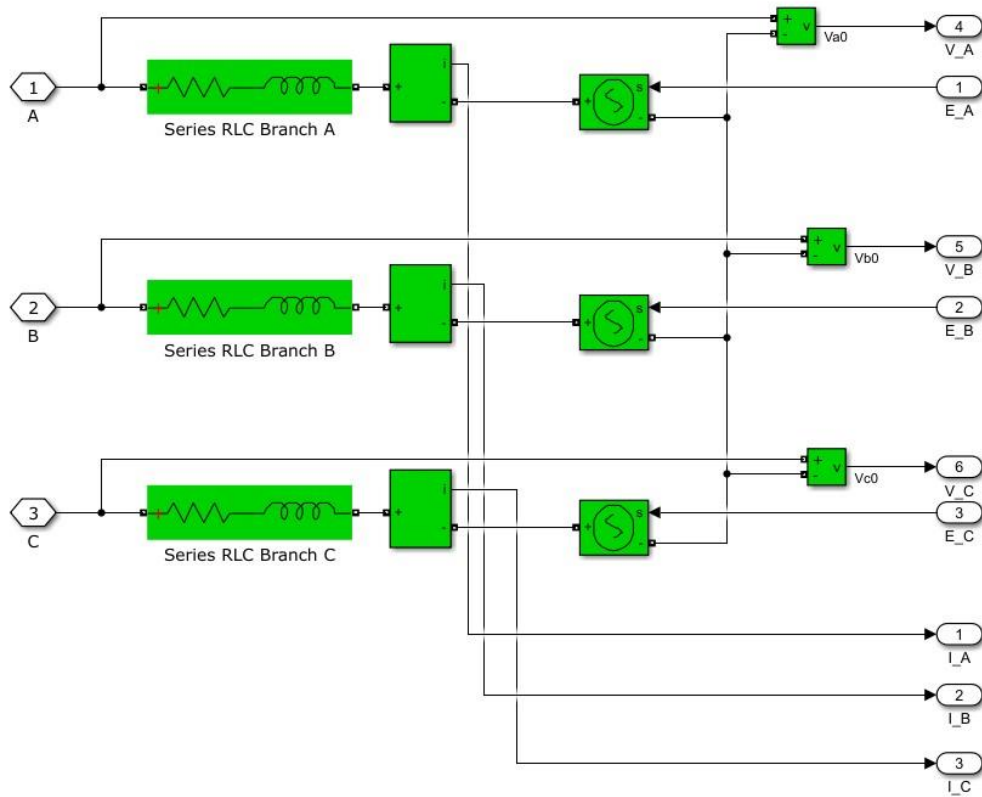


Figure 64: three phase RL subsystem.

Within this subsystem receives on input three currents and the commands from the inverter. Three currents are calculated by multiplying coefficients $K_{f_{cem}}^{(i)}$ and motor's angular velocity to obtain the counter electromotive force (CEF) in the Simulink model called E.

The three phases coming from inverter are now computed using Simscape blocks: Series RLC Branch; this block implements a series of RL elements. Three values of counter electromotive force are used in a Controlled Voltage Source to convert the input signal into an equivalent voltage source. Using current and voltage measurement is possible obtain current and voltage for each phase.

Computation of motor torque

This subsystem provides to compute the motor torque using a multiplication by counter

electromotive coefficients and the current that circulating on each phase, therefore, the final torque is given by a summatory of the contribution of phases:

$$T_M = \sum_{n=1}^3 (k_n \cdot I_n)$$

The saturation block called “saturation” is due to the behavior of the magnetic field inside coils. The electromagnetic field does not increase to infinite value, but it is regulated by a hysteresis cycle.

For iron core that is located in the stator the hysteresis cycle must be very small due to be polarized many times per second, after a polarization when the current goes to zero the iron core must not have a residual polarization according to hysteresis cycle.

In the Figure 65 is represented the computation of motor torque.

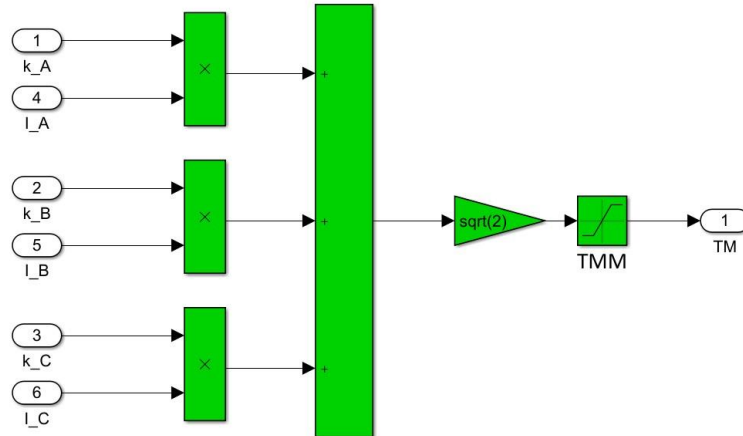


Figure 65: Computation of motor torque.

Material for stator and rotor

To understand this phenomenon, introduce the concept of polarization and how it works:

Inside the ferromagnetic materials there are zone that have the same magnetic moment, in particular, all atoms inside that zone have the same magnetic orientation and are called Weiss domain. A ferromagnetic material, never previously magnetized, it has its own

magnetization on the whole zero, because Weiss domain are randomly distributed.

Current generates a magnetic field, during the passage of current through the coils, the magnetic field causes the Weiss domains rotation and obtain the alignment to the magnetic field. Furthermore, domains walls tend to glide each other causing a possible macroscopic dimension variation of the part; to avoid this phenomenon in stator electric motor is made of Weiss domains are spherical as possible in order to minimize shape variation.

The opposition to changes in the orientation of the domains manifests itself not only when it varies the intensity of the external field impressed, but also if the direction of the latter changes. The reorganization of the domains within a ferromagnetic material follows with delay the variations of the impressed field. This phenomenon, called magnetic hysteresis, occurs in all ferromagnetic materials, and determines their main characteristic, consisting in the ability to retain a resulting magnetic moment even in the absence of an external field. in electric motor there are two main type of ferromagnetic material: soft magnetic materials and hard ferromagnetic materials.

- *soft magnetic materials*

Have a narrow hysteresis loop and values are defined as high permeability (high slope of the average line of the cycle); they offer little opposition to magnetization, in the sense that induction quickly follows the variations of the field: they are suitable for stators. These materials have a low coercive force.

- *hard ferromagnetic materials*

Have a large hysteresis with high opposition to the orientation of the domains in the direction of an external field and subsequent demagnetization. The hysteresis cycle of these materials are large and stocky and in some cases practically rectangular in shape. The characteristic of ferromagnetic materials to remain is more pronounced magnetized even when the external field is zeroed: they are therefore suitable for use as permanent magnets.

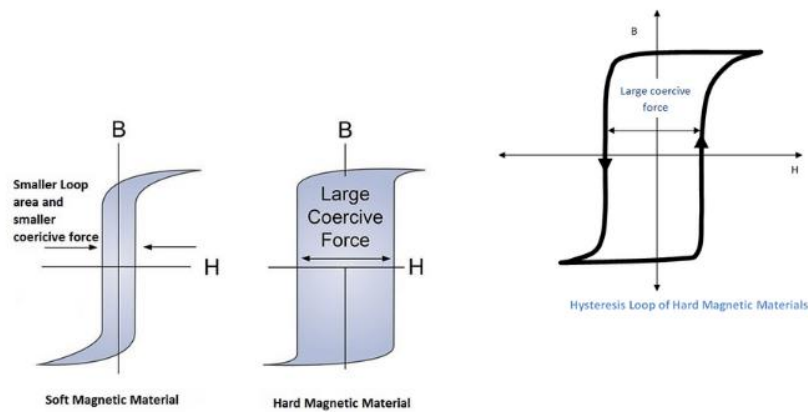


Figure 66: Hysteresis cycle of ferromagnetic materials.

motor-transmission dynamical model

Within this subsystem act the torque of the motor called T_m and the *load*. The values of the load are derived by using test bench, this solution is adopted to improve the high-fidelity model; Using the reverse process, where the command is generated by the high-fidelity model in which the values are assigned to the variable “*load*” that simulates the load values. To carry out the laboratory tests it is necessary to try to recreate the load values generated in the model. Using this process, many errors are entered, first, the difficulty of reproducing the load values exactly on the test bench, this leads to a high discrepancy of the results between the test bench and the MatLab/Simulink model. For this reason, the load values are used the value that derives from test bench measurements.

Load values are multiplied by gear ratio because the application zone of the braking force is located before the gearbox. The Figure 67 below shows how the model is built.

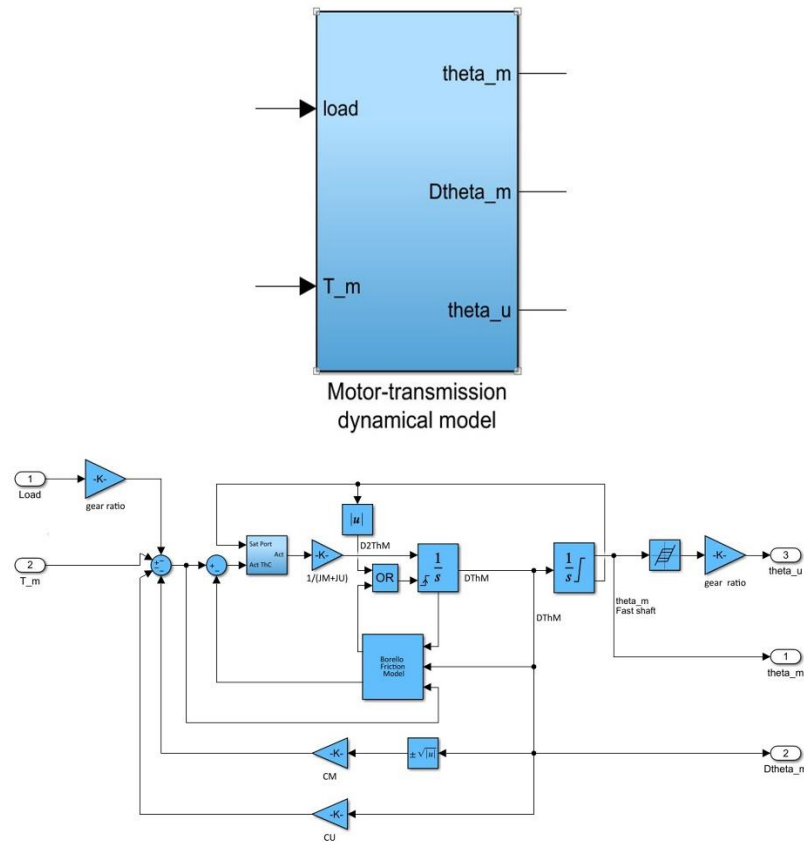


Figure 67: Motor-transmission dynamical model.

The dynamical model uses the motor torque and the load to compute a resulting force that is reduced by the effect of viscous frictional forces, dry friction and the inertia forces. Through integration is possible to obtain the angular position of user, in this Simulink model is implemented the support reaction, the backlash phenomena and the Borello's friction model, on test bench the support reaction is not implemented.

Borello friction model

Modelling friction phenomena is not easy, in literature there are different dry friction models (Classical Friction Model, Dahl's Friction Model and Karnopp's Friction Model) most common models have pros and cons. Borello friction model was developed at the Polytechnic of Turin, a model that represents a fair compromise between other models. The proposed numerical model is satisfactorily adherent to the classic Coulomb friction model and can be easily integrated into more complex calculation programs (for example, to servomechanisms or actuation systems). Borello's model denotes the physical behavior and overcomes other

friction models problems:

- It Discriminates the sign of the friction torque as a function of the direction of the speed.
- It discriminates the possibility the mechanical element stops and the maintenance of the stop condition.
- It discriminates the dynamical and static conditions.
- It evaluates the possibility of the restart of the mechanical element.
- The model takes into account the presence of any limit switch and the consequent impact.

The Borello formulation is expressed as:

$$F_{res} = \begin{cases} F_a & \text{if } v = 0 \wedge |F_{fri}| \leq FSJ \\ FSJ \cdot \text{sign}(F_{fri}) & \text{if } v = 0 \wedge |F_{fri}| > FSJ \\ FDJ \cdot \text{sign}(v) & \text{if } v \neq 0 \end{cases}$$

Where F_{res} is the calculated friction force, FSJ is the value of friction force during static or adherence condition, FDJ is the value of friction force on dynamic condition, F_a is the active force applied to the system, and v is the body speed. To avoid numerical instability Simulink model is equipped by an additional condition:

$$v(t_{i+1}) = 0 \quad \text{if } v(t_{i+1}) \cdot v(t_i) \leq 0$$

This condition provides an effective solution to Karnopp's model. If detects a variation of sign between the actual step time and the previous step time therefore the speed is set to zero at the actual step time.

In the Figure 68 Borello's friction model is presented.

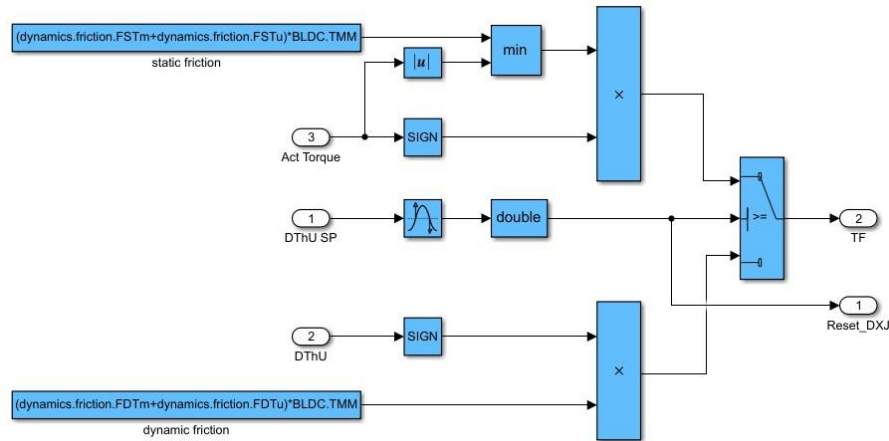


Figure 68: Borello's friction model.

In the "*motor-transmission dynamical model*" the presence of an mechanical limit switch has been implemented; Figure 69 shows how this condition has been applied. Using a dynamic view; the speed is compared with the position, in case an mechanical limit switch is present the position set in saturation and through the saturation port it is possible to set the speed to zero, the model in Figure 69 uses the sign of the speed multiplied by the dynamic friction torque to evaluate the Coulomb friction torque and a switch block to define the torque value. From a static physical point of view, the absolute value of the torque is compared with the static friction torque and using the minimum between these two signals.

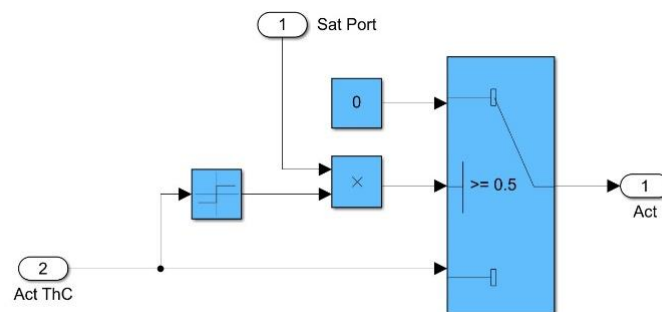


Figure 69: Reaction model.

The first integrator is used for "*zero-crossing-detection*" which is used to have a signal of when the integrator value goes from a positive to a negative value or vice versa. If the zero-crossing-detection block output is equal to 1, it means that the integrator has passed zero,

which means that the static friction branch in the Borello model is activated. To avoid numerical instability problems each time *zero-crossing-detection* detects a zero the speed is reset to zero. If the output is zero it means that the zero-crossing has not occurred and continues to use the dynamic friction model. Within the support reaction subsystem, a comparison with a threshold value takes place. In the case where the motor is in the upper or lower limit position the switch block outputs a zero value, in all other cases the input torque is equal to the output torque of this block.

Signal acquisition

Within this model the three currents of each motor phase are computed using Clark to obtain the equivalent currents I_α and I_β ; Park matrix uses as input the currents computed by Clark matrix and outputs the quadrature current and direct current. For clarity, the currents are filtered by first-order filters to obtain the equivalent current and direct current.

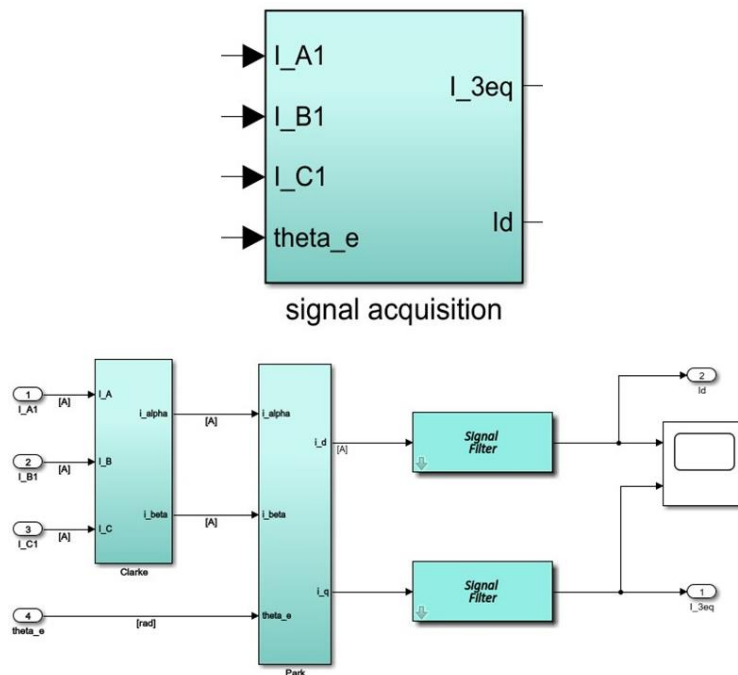


Figure 70: Signal acquisition blocks.

Modification of parameters

Before carrying out the laboratory tests, a number of calibrations are accomplished to

correctly set up both the electric motor and the Simulink model. The settings are also used to obtain the same modelling of the phenomenon studied. In fact, both the test bench and the Simulink model must have a limitation on the maximum number of revolutions and the maximum current; these two limitations are fundamental for obtaining a correct correspondence between models. Using “*TIA portal*” to explore Control Unit settings Simulink model were made:

- *Controller proportional gain*: this proportional operator acts on the position error expressed in radians; its value has been calibrated to the value present in the test bench:

$$Controller.Gprop = \frac{1000}{60} \cdot 124$$

Where “124” represents the conversion to fast shaft and then the transmission ratio.

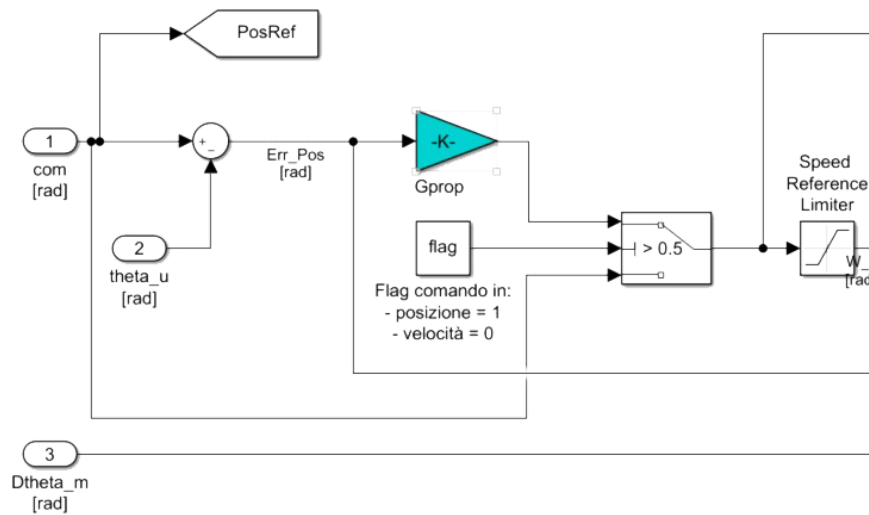


Figure 71: Modified Proportional gain.

- *Error position saturation*: There is a motor speed limitation inside the motor control unit. This limitation is inserted to protect the motor from high currents:

$$controller.W_{refMax} = 500 \cdot \frac{\pi}{30}$$

The modified Simulink block is shown in Figure 72:

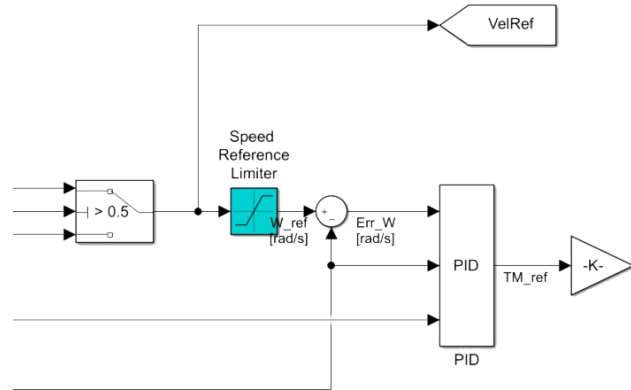


Figure 72: Modified Speed reference limiter.

- *Current Reference Limiter:* This limitation is inserted to protect currents in order to avoid generating high currents. This protection also useful to eliminate any current peaks that could otherwise burn out the motor; this value has been set at 22,5 Amps.

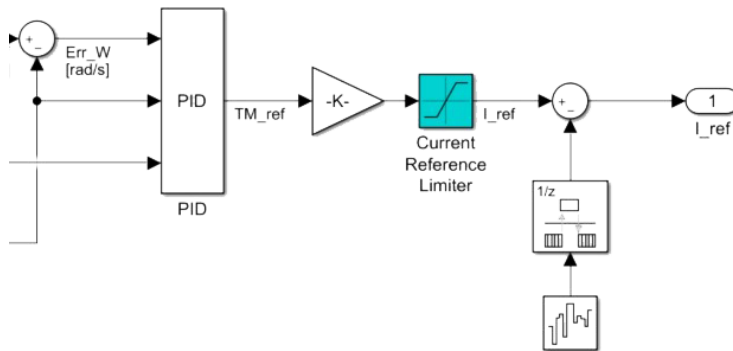


Figure 73: Modified Current Reference limiter.

- *Planetary gearbox momentum of inertia:* In order to correctly assess the behavior of the planetary gears, the inertia of each stage is studied. Using Solidworks tools, the moment of inertia of the planetary gearbox is evaluated at 0,00190504 kgm². In the Simulink model, the moments of inertia of the motor and the user are added together.

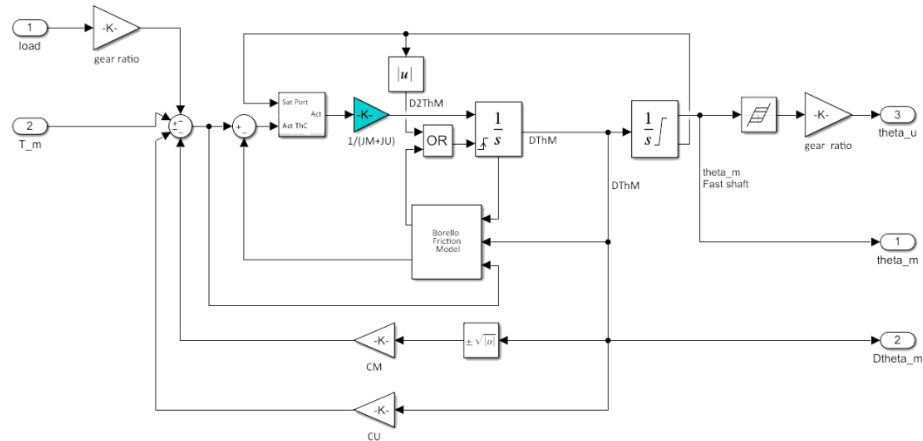


Figure 74: User inertia moment.

Backlash evaluation

In this section it presents the first results obtained from the test bench. In order to set the correct parameters in the Simulink model, the backlash evaluations were conducted with the engine switched off. Using “*Starter*” software it recorded encoder position as the position of the manual precision positioner changed. The encoder backlash evaluation was recorded considering the total backlash amplitude; the experimental data were then compared with the data obtained from mathematical calculations. The results are shown in the next table.

	Horizontal distance	wheelbase spacing	Diff radial spacing	Backlash calculated		Sperimetal backlash	
	[mm]	[mm]	[mm]	[rad]	[°]	[rad]	[°]
1	14	108,43	0	0,0000	0,0000	0,0064	0,3656
2	13,8	108,57	0,14	0,0012	0,0661	0,0087	0,1336
3	13,5	108,78	0,35	0,0029	0,1653	0,0094	0,1751
4	13,3	108,92	0,49	0,0040	0,2316	0,0112	0,2765
5	13,1	109,06	0,63	0,0052	0,2980	0,0120	0,3226
6	12,8	109,27	0,84	0,0069	0,3978	0,0143	0,4562
7	12,4	109,55	1,12	0,0093	0,5311	0,0172	0,6175
8	12	109,83	1,40	0,0116	0,6647	0,0193	0,7419
9	11,5	110,19	1,76	0,0145	0,8322	0,0227	0,9354
10	11	110,54	2,11	0,0175	1,0003	0,0265	1,1520
11	10,5	110,90	2,47	0,0204	1,1689	0,0300	1,3548
12	10	111,25	2,82	0,0234	1,3381	0,0348	1,6266
13	9,5	111,61	3,18	0,0263	1,5077	0,0401	1,9308
14	9,15	111,86	3,43	0,0284	1,6268	0,0436	2,1335
15	9	111,97	3,54	0,0293	1,6779	0,0457	2,2533

These measurements were carried out by varying the position of the manual precision positioner (column 1 on the previous table) and measuring the backlash on the encoder.

Mathematical calculation of the backlash was carried out by assuming two horizontal racks with equal pitch and module at the last stage of the planetary gear and the gear mounted on the encoder, the backlash is given by the distance between the two racks. The mathematical formula used is as follows:

$$Backlash = \frac{\Delta_{radial\ spacing} \cdot \tan(20^\circ)}{88} \cdot 2$$

This formula allows the number of teeth of the last stage of the planetary gearbox and the tooth module to be taken into account. $\Delta_{radial\ spacing}$ this difference is obtained by subtracting the initial position of the manual precision positioner from the current position.

The graph below shows the position of the manual precision positioner on the X axis and the gear backlash on the Y axis. It can be seen that for small values of backlash the calculated values and the experimental values are very similar; for high values the two measurements

deviate; the region of this can be found that the involute profile with which the gears were constructed is not a precise profile but is approximate.

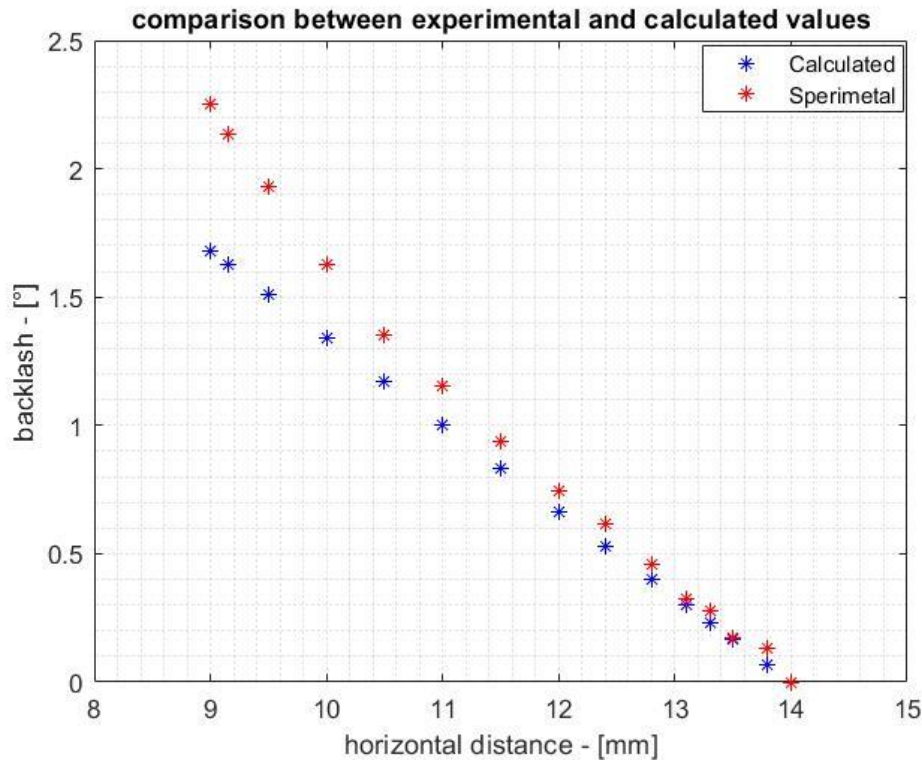


Figure 75: Comparison between calculated and sperimental gear backlash.

Testing campaign

The first test campaign is carried out with a sinus command of $7,0^\circ$ amplitude, $10,0^\circ$ bias and a frequency of 0,2 Hz given via web server to the test bench. The data acquisition systems of the bench test were two:

- Starter software: In this program it is possible record position, speed and current data of the motor and the closed-loop control system. The recorded values are as follows:

Xms: Time [msec]

C0Drive_axis_1r4821 = Encoder position rapported to fast shaft

C1Drive_axis_1r4820 = motor shaft position rapported to fast shft

Drive_axis_1.r62 = command speed [rpm]

Drive_axis_1.r63 = read speed

Drive_axis_1.r77 = Current setpoint torque-generating

Drive_axis_1.r76 = Current actual value field-generating
Drive_axis_1.r1733 = Quadrature-axis voltage setpoint
Drive_control.r722 = Trigger signal

- MatLab/Arduino board: scripts used to record the values of the load cell placed on the brake, in these tests the brake was not operated. The Arduino board performs a signal synchronization through a "Trigger" signal sent to the motor control unit. MatLab code generates a file that contains on the first column the time values and on the second column the read values of the load cell.

The test campaign has analyzed the behavior of the test bench at the backlash variation, in particular the tests have been carried out at the increase of gear backlash. Other test campaign was realized using braking module and it was possible to apply a braking torque to the motor shaft.

After it has been possible to compare the results of the bench test with the results of the simulation in MatLab/Simulink.

Results

The analysis between the laboratory tests and the Simulink model results made it possible to validate the model under gear backlash conditions. In particular for small values of gear backlash. In the following, the behavior under nominal conditions of minimum gear backlash is analyzed. The first laboratory test resulted in finding that there is initial and uncontrollable gear backlash. The native gear backlash is caused by coupling errors during the assembly phase, tolerance errors during the parts printing phase. Finally, it is noted that the constant backlash present in all laboratory tests is 0,3656 radians. The initial position of the manual precision positioner is set at 14,00 mm, so that there is no backlash on the gear.

Figure 76: Simulink, Test bench and command encoder position
Figure 76 shows the encoder position recorded by the test bench and the encoder position calculated by the Simulink model. It is possible to see that the two models are very similar, the Simulink model

succeeds very well in reproducing the behavior of the test bench with zero backlash on the encoder.

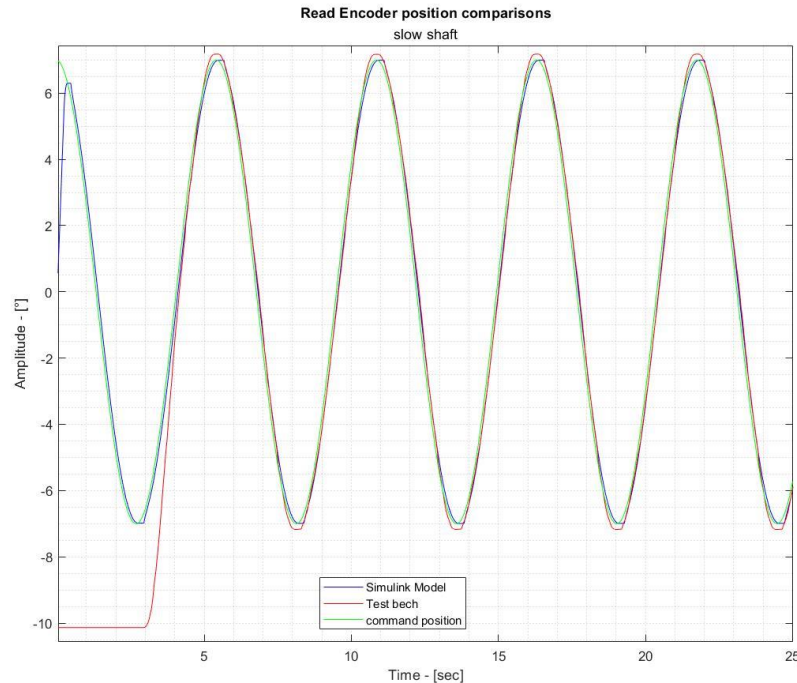


Figure 76: Simulink, Test bench and command encoder position.

The graph shows with green line the position commanded with a frequency of 0,2 Hz, amplitude equal to 7,0 degrees, the position of the test bench encoder is defined by the red curve, the blue sinusoid indicates the position of the encoder in the Simulink model. This comparison shows that the Simulink model correctly simulates the encoder position. The transient regimes have not been considered due to the complexity of modeling, the data analyzed and the conclusions obtained refer to strokes in which the sinusoids command has reached an equilibrium and all transients in the test bench have been exhausted. By comparing the positions of the user, in particular, analyzing a peak in a sinusoid period it is possible to see the presence of internal backlash: the red horizontal curve represents the internal gear backlash, present inside planetary gears, while the blue curve represents the gear backlash modeled through measurements and implemented with a constant contribution in the gear backlash block.

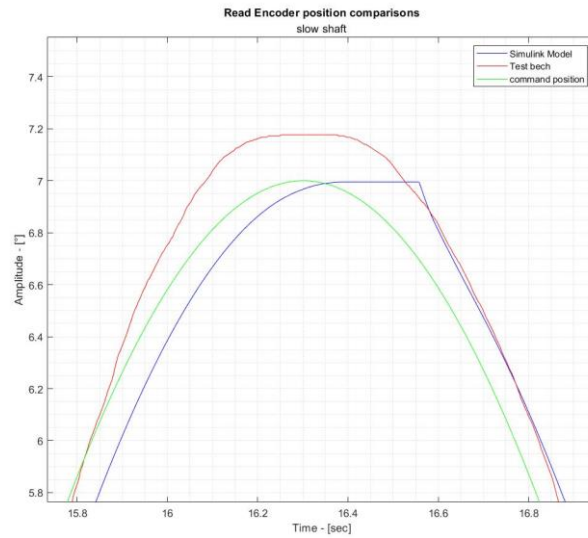


Figure 77: Differences between test bench and Simulink model.

The positions of the motor are represented in Figure 78, it see that also in this case the position of the sine wave created by the test bench has a greater amplitude than the sine wave created by the Simulink model.

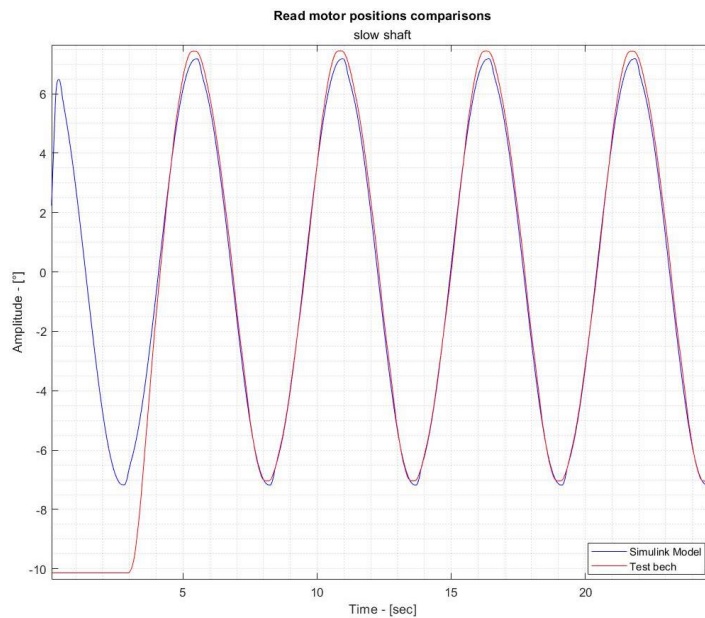


Figure 78: Comparison of motor positions.

The major differences between the Simulink model and the bench test lie in the amplitudes of the sine waves. The main reason why these values are different could be traced to the reconstruction of the command.

The command given as input to the Simulink model comes to an approximation of the data obtained from the test bench. During the test campaign it was not possible to measure the command actually provided to the control unit. To avoid this, it was decided to reconstruct the command through the speed measured by the test bench. To obtain the command position it was necessary to divide the position by a gain. The value of the gain is the same both in the Simulink model and in the Control Unit system control, equal to $G = \frac{1000}{60} \cdot 124$.

A function was written, that uses the phase and frequency of a sine wave as input and calculates the integral of the error between the sine function and the position command reconstructed from the velocity. The objective for the construction of the command, to be provided as input to the Simulink model, is to find phase and frequency, MatLab function "*fmincon*" uses as input the function described above and varies the phase and frequency in order to minimize the error. This function allows to synchronize the signals perfectly and with the minimum possible error, here below are represented with green line the encoder position and black line the sinusoid built minimizing the error, for completeness are shown the synchronization tests with zero gear backlash and the test with maximum gear backlash in order to verify the general validity of these functions.

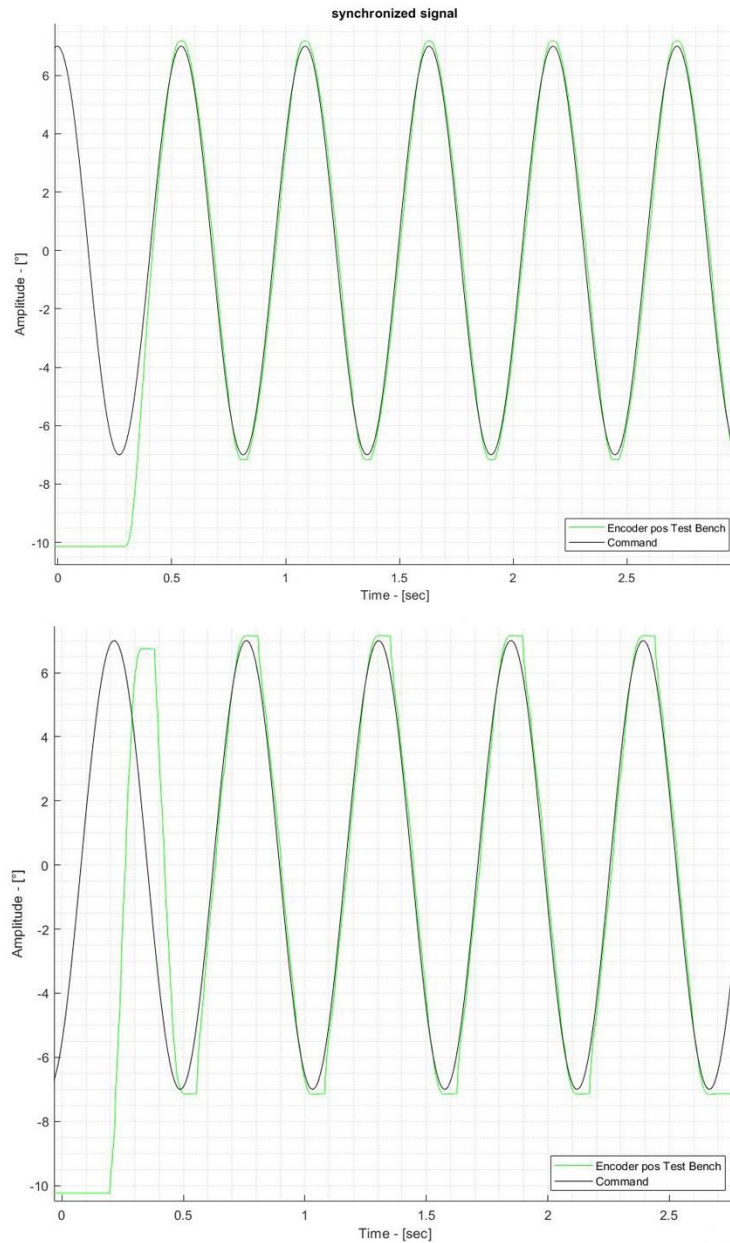


Figure 79: Above Encoder with zero backlash and below planetary gearbox with maximum gear backlash.

As can be seen from the graphs above, the values recorded by the bench test have an amplitude slightly higher than the actual amplitude commanded. This phenomenon could be traced back to the control logics implemented inside the control unit. If an analysis of all the data is carried out, it is possible to obtain the error between the positions of the bench test and the Simulink model. The graphs show that when the gear backlash varies the error committed remains constant, in first approximation; this fact leads to the conclusion that the difference noted between the amplitudes of the signals can be corrected by inserting

multiplicative coefficients in the Simulink model. The Figure 80 and Figure 81 show the error made as the variation of the gear backlash.

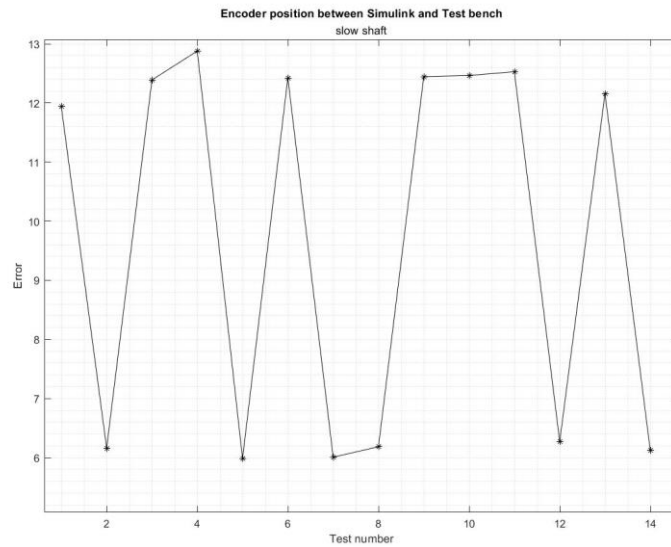


Figure 80: Position Encoder error.

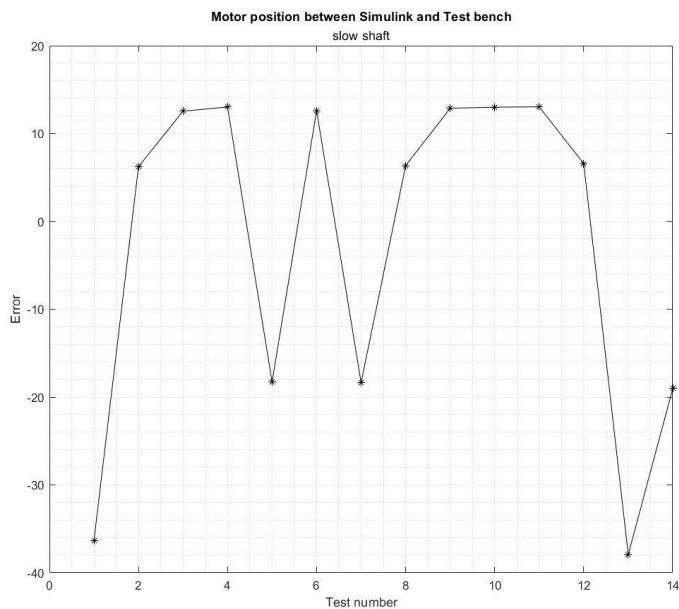


Figure 81: Position motor error.

An additional verification was performed on the speeds. The speeds used to make the comparison are: the speed read by the encoder of the motor of the test bench and the output

speed of the dynamic motion transmission model. It can be seen from the graph that for both low and high gear backlash the model can follow the speed measured in the test bench.

from the Figure 82 it can be seen that during the transient periods the model does not follow the behavior of the bench test. analyzing the behavior after 10 seconds it can be seen that the Simulink model reproduces the behavior of the bench test speed. the comparison is made with zero gear backlash, average gear backlash and maximum gear backlash values.

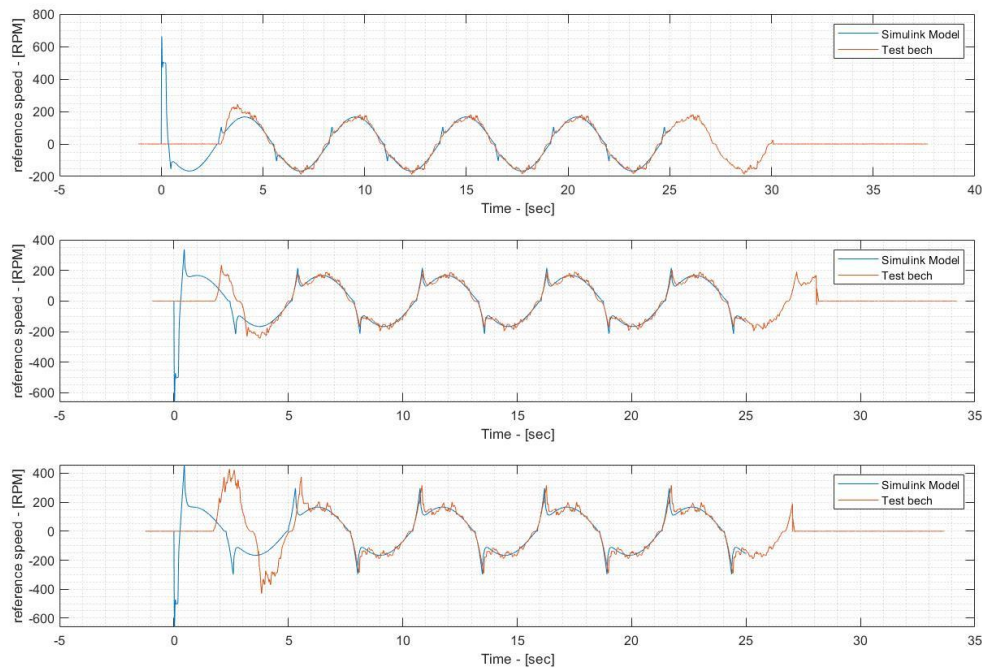


Figure 82: Speed comparisons.

Finally, the comparison in Figure 83 of the user positions led to the conclusion that the Simulink model can truthfully simulate the behavior of the bench test under conditions of gear backlash. As it is possible to see from the Figure 80 error committed in the approximation of the position is constant as the gear backlash varies, a variation of the gains of the Simulink model can lead to increase the performance of the model and bring it closer to the data obtained from the test campaign.

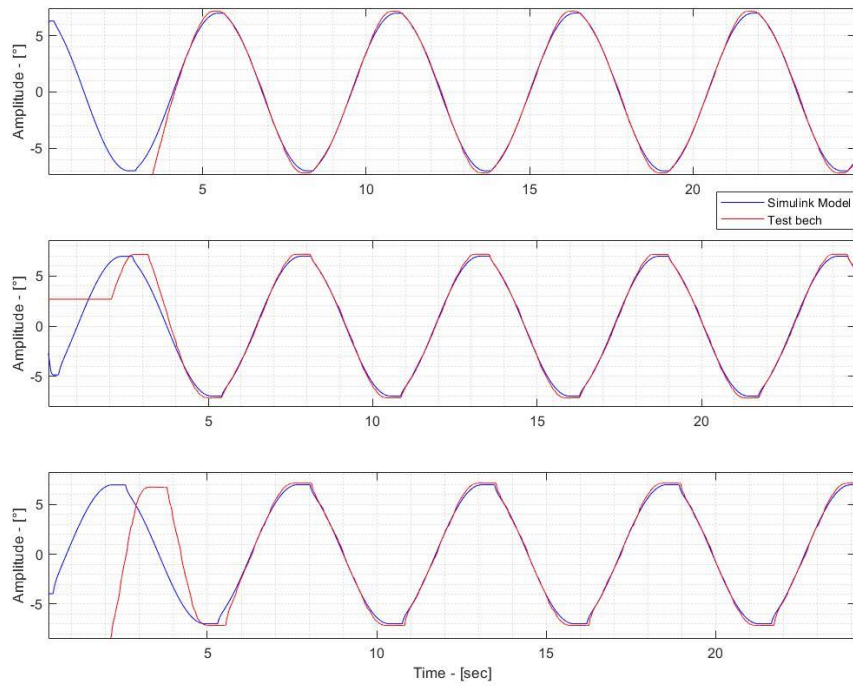


Figure 83: Minimum, medium and maximum gear backlash on last stage of the planetary gearbox.

Variable load test campaign

The testing campaign continued with tests with variable shaft load and variable gear backlash. The load values applied by the brake module were sized between values of 0.2 Nm and 2 Nm; the maximum braking torque value developed by the brake module was chosen on the basis of the maximum torque developed by the motor and using a safety coefficient to avoid motor breakage. Once a gear backlash condition is fixed, the torque applied to the motor shaft is varied; a linear distribution is assumed between the minimum value of applied braking torque and the maximum value.

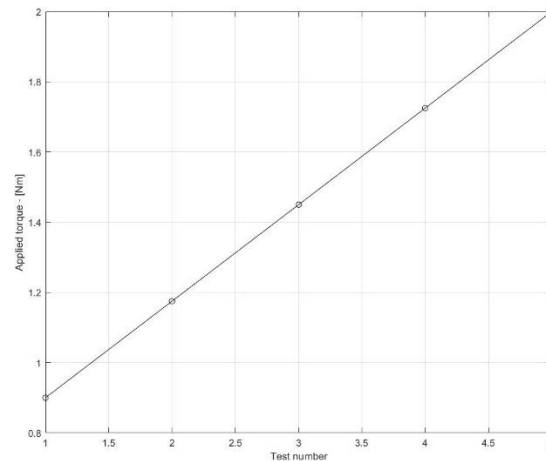


Figure 84: Linear distribution of torque tests.

The backlash values used were three reference values:

- Zero backlash $\Rightarrow 0,0$ rad
- Medium backlash $\Rightarrow 0,0145$ rad
- Maximum backlash $\Rightarrow 0,02335$ rad

These three values were chosen because they are the limits of values for which experimental gear backlash measurements and mathematical calculations are sufficiently approximate with minimal error as seen from the Figure 75.

The Servo Motor Actuation System is based on closed loop control and the Arduino board modulates the signal to the servo motor to try to keep the value read from the load cell constant, and equal to the value provided as input by the user.

This test campaign required the modulation of a different input to the test bench. In order to exhaust all transient phenomena during the braking phase it was necessary to increase the amplitude of the sine wave, to prevent the currents supplied to the motor reach saturation the frequency was lowered.

The input values obtained through web server are:

- Amplitude: 45°
- Frequency: 0,05 Hz
- Bias: 60°

Future trends

This thesis is one of the beginning issues for a new develop of maintenance. New conception of maintenance is necessary for a cost-effective project, in particular the predictive maintenance is could be improved by real time models through flight data and data given from sensor already installed. In this way is possible monitor all components condition and take action if necessary. For example: Ailerons wear conditions. In this case if an actuator of one aileron is more wear than others is possible give same maneuver by a combination of other mobile surfaces. In this way is possible to obtain a uniform wear of all actuator and sell in maintenance the aircraft only once time for a lot of maintenance and not for one.

The main objective of this work is to get the bench test up and running and make it easy to implement. The first goal achieved was to close the position loop through the encoder placed on the last stage of the planetary gear. An important milestone was to give the possibility to the user to give commands via web server; this improvement has required a substantial modification of the internal software of the control unit and the PLC, the adoption of a web server system has made possible the operation of the test bench without the installation of additional programs; it is still essential to use the "*Starter*" software for data recording. The characterizations carried out in previous works have made it possible to set the gains of the Simulink model. After the characterization of the test bench in nominal conditions it was possible to analyze on malfunctioning conditions, the case analyzed is that of gear backlash, in the future it is possible to characterize the motor also in conditions of failure, such as in the case where a winding of the three phases of the motor does not work at 100% but there is a small short circuit between the windings and then the chained flux created by the coils are reduced. An important development for the characterization of the bench test is to insert an inertia on the toothed wheel positioned on the encoder, to simulate the inertia of a moving surface. This mass increase could be realized by inserting a lead mass on the outer surface of the gear wheel to shift the center of gravity away from the axis of rotation.

Bibliography

- [1] N. S. Nise, *Controlli automatici*, P. Pugliese, A cura di, Novara, Italia: Città Studi Edizioni, 2013.
- [2] L. Frosini, *Analisi delle Vibrazioni per la Diagnostica delle Macchina Rotanti*, Pavia, Italia: Dipartimento di Ingegneria Industriale e dell'Informazione.
- [3] S. Taşkin, S. Şeker, I. Çankaya e M. Akar, «Detection of static eccentricity for permanent magnet synchronous motors using the coherence analysis,» *Turkish Journal of Electrical Engineering and Computer Sciences*, p. 13, 4 October 2016.
- [4] L. Hongxin, «Stator Magnetic Core Brushless Motor Apparatus, System And Methods». Unites States Brevetto US 2017/0288478 A9, 5 10 2017.
- [5] «SIEMENS - Industry Online Support - Product Support - Operating Instructions,» [Online]. Available: [https://support.industry.siemens.com/cs/products/6ag4141-.....-..../simatic-ipc427e-\(microbox-pc\)?pid=809428&mlfb=6AG4141-.....-....&mfn=ps&lc=it-IT](https://support.industry.siemens.com/cs/products/6ag4141-.....-..../simatic-ipc427e-(microbox-pc)?pid=809428&mlfb=6AG4141-.....-....&mfn=ps&lc=it-IT). [Consultato il giorno 20 05 2021].
- [6] «Control Unit CU310-2 PN (PROFINET) Manual,» [Online]. Available: https://cache.industry.siemens.com/dl/files/000/99673000/att_51983/v1/GH6_0414_eng_en-US.pdf.
- [7] «SINAMICS - SINAMICS G120 frequency converters - PM240-2 Power Modules - Hardware Installation,» [Online]. Available: https://cache.industry.siemens.com/dl/files/315/109750315/att_929650/v1/G120_PM2402_hw_inst_man_0817_en-US.pdf.

- [8] AIRBUS, «Global Market Forecast -Cities, Airport & Aircraft 2019-2038,» Blagnac Cedex, France, 2019.
- [9] L. Andre, «BOEING 737 SYSTEMS REVIEW».
- [10] G. Jacazio e S. Pastorelli, *Meccanica Applicata alle Macchine*, Torino, Italia: Levrotto & Bella, 2001.
- [11] MOOG, «Aircraft Electromechanical Actuators,» MOOG, [Online]. Available: <https://www.moog.com/products/actuators-servoactuators/actuation-technologies/electromechanical/aircraft-electromechanical-actuators.html>. [Consultato il giorno 26 06 2021].
- [12] H. Ligang, Y. Tian, Z. Jiao e Y. Li, «Active Load-Sensitive Electro-Hydrostatic Actuator for More Electric Aircraft,» *applied sciences*, p. 21, 6 10 2020.
- [13] K. Bahadır, Y. Nihat, . F. Erdoğan e M. Vardar, «A study on prediction & validation of meshing gear pair backlash,» 2019.
- [14] P. Maggiore e M. D. L. Dalla Vedova, *Dispense e appunti Corso di Modellazione e simulazione di sistemi aerospaziali*, Torino, Italia, 2020.
- [15] P. Maggiore e M. D. L. Dalla Vedova, *Dispense e appunti corso di Sistemi di Bordo aerospaziali*, Torino, Italia, 2020.
- [16] ItalSensor Company, [Online]. Available: <http://www.italsensor.com/en/tsw58/>. [Consultato il giorno 04 07 2021].
- [17] V. Boschetti, *Development of an Experimental Test Bench for the Validation of Prognostic Algorithms for Electromechanical Actuators*, 2020.
- [18] P. Sciandra, *Development and Validation of Prognostic Algorithms for Electromechanical Actuators*, 2020.